A review of breast tomosynthesis. Part II. Image reconstruction, processing and analysis, and advanced applications

Ioannis Sechopoulos[a)]
Department of Radiology and Imaging Sciences, Hematology and Medical Oncology and Winship Cancer Institute, Emory University, 1701 Upper Gate Drive Northeast, Suite 5018, Atlanta, Georgia 30322

(Received 13 June 2012; revised 16 November 2012; accepted for publication 16 November 2012; published 4 January 2013)

Many important post-acquisition aspects of breast tomosynthesis imaging can impact its clinical performance. Chief among them is the reconstruction algorithm that generates the representation of the three-dimensional breast volume from the acquired projections. But even after reconstruction, additional processes, such as artifact reduction algorithms, computer aided detection and diagnosis, among others, can also impact the performance of breast tomosynthesis in the clinical realm. In this two part paper, a review of breast tomosynthesis research is performed, with an emphasis on its medical physics aspects. In the companion paper, the first part of this review, the research performed relevant to the image acquisition process is examined. This second part will review the research on the post-acquisition aspects, including reconstruction, image processing, and analysis, as well as the advanced applications being investigated for breast tomosynthesis. © *2013 American Association of Physicists in Medicine*. [http://dx.doi.org/10.1118/1.4770281]

Key words: breast tomosynthesis, digital mammography, breast cancer, review, image reconstruction, image processing, image analysis, contrast enhanced imaging, radiotherapy, elastography, phase contrast

I. INTRODUCTION

The companion paper provided a review of the medical physics research performed on all aspects of the digital breast tomosynthesis (DBT) image acquisition process. This paper will review all relevant post-acquisition aspects, including image reconstruction, artifact reduction, and other image processing and analyses, in addition to reviewing the research performed on advanced applications and implementations of DBT, including multimodality imaging, in which DBT is combined with other imaging technologies.

II. TOMOSYNTHESIS RECONSTRUCTION

An in-depth overview of the history and principles of tomosynthesis reconstruction algorithms has been previously published by Dobbins and Godfrey,[1] so these aspects will not be discussed here. This discussion will be focused on the different reconstruction methods currently in use or under development in DBT, and the many improvements for each that have been proposed lately.

II.A. Filtered backprojection

The most commonly known analytical algorithm for tomosynthesis reconstruction is filtered backprojection (FBP), normally used in computed tomography (CT). As in CT, the choice of filters applied to the projection data before the backprojection is performed can drastically affect the quality of the reconstruction. Mertelmeier *et al.* presented a general theory for FBP applied to DBT with linear (or arc) x-ray tube motion, in which, in addition to the usual ramp-type and apodization filters, the authors introduce a slice thickness filter that dampens the impact of the incomplete sampling of the frequency space due to the limited angular range used in tomosynthesis, therefore controlling the impact of out-of-plane artifacts on image quality.[2] By deriving, validating and using a three-dimensional (3D) cascaded linear system model for DBT, Zhao *et al.* determined, among other results, that the use of this slice thickness filter reduces aliasing and improves 3D DQE.[3,4] Using task-based analysis, Wang *et al.* showed a small improvement in mass detectability in the central slice of the lesion, but qualitatively found a decrease in out-of-plane artifacts.[5] Orman *et al.* introduced the concept of an additional filter to avoid the zeroing out of the low frequencies by the ramp filter, thereby introducing an undesirable "flatness"[6] to the image.[7] The resulting modification of the ramp-type filter was clearly shown by Zhou *et al.* (Fig. 1).[8]

II.B. Iterative reconstruction algorithms

Attempting to combine the benefits of an iterative reconstruction method [the simultaneous iterative reconstruction technique (SIRT); Ref. 9] with the speed of FBP, Ludwig *et al.* estimated the impulse response of SIRT reconstruction in DBT and used it to develop a filter in the frequency domain that could be combined with the other filters used to preprocess the acquired projections before backprojection in FBP.[10] This filter, which was found to be weakly projection angle dependent, could be fit to a fourth-order polynomial, yielding a smooth function. The authors found that the use of this filter with FBP results in an important modification of the characteristics of the reconstructed images. Whereas the FBP images present a reduction of the low frequency contrast, resulting in decreased visualization of large area contrast of dense tissue, the images with this iterative-based filter have an overall feel more similar to standard mammograms. In contrast, however,

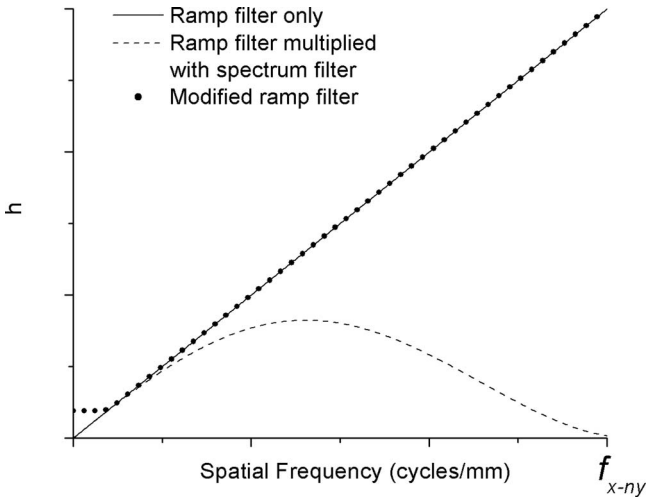

FIG. 1. Modification of ramp filter to maintain the low frequency information in FBP reconstructed DBT images. Reprinted with permission from Zhou *et al.*, "A computer simulation platform for the optimization of a breast tomosynthesis system," Med. Phys. **34**(3), 1098–1109 (2007). Copyright © 2007, American Association of Physicists in Medicine (AAPM).

the excellent skin line visualization and sharpness of FBP is somewhat lost with the application of this filter.

In a study relevant to any DBT reconstruction algorithm involving backprojection, Chen *et al.* investigated the impact of the x-ray tube moving in an arc during acquisition while using a traditional shift-and-add (SAA) type algorithm for backprojection, in which the pixels are shifted only in the direction parallel to the x-ray tube motion.[11] As shown by the authors, the slight but non-negligible shift in the projection of each voxel in the direction perpendicular to the tube motion needs to be taken into account to avoid blurring of fine features, which is especially important in the characterization of morphology of microcalcifications.

In a different implementation of FBP, Claus *et al.* proposed that the pre-backprojection filtering be performed taking into account the size of the features included in the projections, with dimensionally dependent filtering. This method of filtration, combined with an order statistics based algorithm for out-of-plane artifact reduction, was shown to yield results similar to iterative reconstruction methods but with a substantial decrease in computation time.[12]

Various algebraic methods have been investigated for the general problem of reconstruction. In general, these methods set up a system of simultaneous linear equations, and differ in how this linear algebra problem is solved using iterative methods, such as the algebraic reconstruction technique (ART),[13] the SIRT,[14] and the simultaneous algebraic reconstruction technique (SART).[15] Zhang *et al.* implemented the SART method for DBT imaging and compared it to standard backprojection (BP) using both homogeneous and structured phantoms.[16] While BP performed similarly or better than SART for some lesions in one of the homogeneous phantoms tested, for the more realistic structured phantom the latter yielded better results, both in terms of in-plane image quality and vertical resolution. Lu *et al.* have proposed two different methods of noise regularization for SART to improve microcalcification visibility without affecting mass detail visibility: one based on selective diffusion[17] and, more recently, another based on wavelet decomposition for multiscale regularization.[18]

A different algebraic reconstruction method, matrix inversion tomosynthesis (MITS), was introduced for DBT by Chen *et al.*[19] MITS was shown to be good at removing out-of-plane artifacts and handling high frequency information, but was also shown to perform poorly with low frequency information.[20] To ameliorate this, Chen *et al.* proposed a hybrid reconstruction algorithm that incorporates the high frequency response of MITS and the good low frequency behavior of FBP, and denoted it Gaussian frequency blending (GFB).[20] With GFB, the authors were able to obtain reconstructed images with improved representation of high frequency signals, e.g., microcalcifications, with enhanced representation of the overall breast tissue characteristics, avoiding the commonly found "flat" breast image in which large area density information is lost.

Other iterative reconstruction methods consisting of two steps per iteration, in which the tomosynthesis acquisition process is modeled in a forward step and the reconstructed object is updated in a backward step, have also been proposed for DBT. The most commonly studied method in DBT is the maximum likelihood expectation maximization method (MLEM) Ref. 21 introduced for DBT by Wu *et al.*[22]

With most iterative reconstruction methods, the computer processing time required to perform the reconstruction is a concern. Wu *et al.* discussed that after two to three iterations detailed features are conspicuous, and that radiologists communicated satisfaction with the results after eight to ten iterations, with no further improvement in image quality after ten iterations.[22] In early developments, a method to accelerate the MLEM reconstruction algorithm was proposed by Wu *et al.* in which the reconstructed volume is broken up into oblique sections that can be reconstructed by separate threads of a multiprocessor computer or multiple nodes of a computer cluster.[23] This method was then modified for implementation with graphics processing unit (GPU)-based hardware.[24] With the advances in this type of hardware, including an ever-increasing number of computing cores and amount of memory,[25] the reconstruction time has continued to drop, rendering the many "tricks" needed to avoid the memory issues encountered in the early implementations unnecessary. Implementations of some iterative algorithms optimized for running on a workstation-level GPU card can now just take a few seconds per iteration for a complete patient breast case.

In studying the order in which the acquired projections are processed in each iteration by iterative methods, Wu *et al.* found that the use of sequences other than that matching the acquisition order can substantially improve the resulting reconstruction quality.[26] In this study, the authors used a modified ML-convex algorithm that uses pairs of projections at a time to modify the reconstructed volume, and they found that all three different ordering schemes investigated result in image quality improvement compared to the conventional ordering.

II.C. Novel reconstruction methods

Many additional novel reconstruction algorithms have been proposed for DBT with varying levels of testing, success, and continued development. Given their infancy, most of these algorithms are not yet used in any system that is commercially available or close to this stage. Among the proposed algorithms, there are algorithms based on total variation regularization,[27,28] total p variation regularization,[29–31] joint entropy regularization,[32,33] adaptive diffusion regularization,[34] iterative penalized maximum likelihood (especially to improve microcalcification visibility),[35] iterative maximum *a posteriori* statistical reconstruction,[36] and Bayesian inference.[37] In a very different approach, Wu *et al.* proposed a reconstruction algorithm that results in spherically symmetric "voxels" as opposed to the traditional cubic voxel.[38] Another algorithm proposes a spectral reconstruction, in which the polychromatic nature of the x-ray beam is taken into account by inputting the spectrum used for acquisition and the algorithm accounts for the variation in tissue attenuation with x-ray energy and beam hardening.[39]

II.D. Comparison of reconstruction algorithms

Many studies have focused on comparing the capabilities of the various reconstruction algorithms proposed for DBT. The two earliest studies to perform a comparison of reconstruction algorithms were published by Suryanarayanan *et al.*[40,41] In the first study, using a custom-made structured phantom, the authors compared the acquired projections to the reconstructions obtained with four reconstruction algorithms: tuned-aperture computed tomography (TACT)-backprojection, iterative TACT, an expectation maximization iterative method and a Bayesian-based iterative method.[40] For the comparison, Suryanarayanan *et al.* performed a contrast-detail (CD) study with five radiologists specializing in mammography. The authors found that all reconstructed images result in better CD characteristics than the projections, and that the reconstructions from projections acquired with higher exposure are better than those acquired with lower exposure. CD characteristic comparison among the tomosynthesis reconstruction methods was not performed. In the follow-up study in which the projections were compared to the TACT-backprojection algorithm and the nonlinear TACT-maximization and TACT-minimization algorithms, the authors again found significantly better CD characteristics for all tomosynthesis reconstructions compared to the projection images.[41] Among the reconstructions, the TACT-backprojection was only marginally statistically better than the TACT-maximization, with all other algorithm differences not being statistically significant. In another comparison study, Wu *et al.* tested the standard BP, filtered backprojection and the iterative MLEM reconstruction methods.[42] Using phantoms and patient images, the authors found that the BP algorithm resulted in the best in-plane image quality of low contrast, larger features, but suffered from out-of-plane artifacts. The FBP algorithm, as expected, performed better than BP for high frequency features. Finally, the MLEM algorithm provided a good balance of image quality between the low and high frequency features. A comparison of the noise power spectra (NPS) of the SAA, FBP, and MITS algorithms by Chen *et al.* showed MITS performed best at middle frequencies, while FBP did better at high frequencies, due to the Hamming and Gaussian low pass filters used.[43] Zhou *et al.* compared the detectability of a low contrast lesion in a simulated breast reconstructed with the EM, SART, and BP algorithms with five human observers and found that the EM algorithm had the superior detectability, with SART being somewhat inferior and BP being very inferior.[44] Rakowski *et al.* compared the BP algorithm, with and without an iterative subtraction (IS) algorithm, and an algebraic reconstruction (AR) algorithm.[45] Using objective metrics for image quality, the authors found that the BP with the IS algorithm resulted in the highest SNR, but the AR algorithm resulted in the highest normalized signal difference and the best ASF. In another comparison study, Zhang *et al.* compared the BP, SART, and MLEM algorithms using breast phantoms.[46] For both iterative methods, the authors used the result of the BP reconstruction as the initial guess of the reconstructed volume, to improve computational efficiency. When using homogeneous phantoms, the BP algorithm resulted in reconstructions with lower noise and higher CNR, while the iterative methods were superior in all other image quality metrics studied. In particular, with clinically more relevant structured phantoms, BP was again found to lack the ability to reduce out-of-plane artifacts, while both SART and MLEM did reduce these artifacts. In general, SART and MLEM resulted in very comparable image quality, but SART was found to require fewer iterations than MLEM to achieve these results. Zhou *et al.*, as part of a larger study, compared FBP and MLEM using computer simulations and concluded that although MLEM consistently outperformed FBP, the latter can achieve comparable image quality to the former with an optimized acquisition geometry and reconstruction filter.[8] Bliznakova *et al.* used monochromatic synchrotron radiation to image a custom-made structured breast phantom and compared four reconstruction methods: the multiple projection algorithm (MPA, equivalent to BP),[47] FBP with a ramp filter and with a ramp and hamming window, and the MPA with noise mask subtraction algorithm[48] (MPA-NM).[49] Overall, the MPA-NM method was found to be superior due to it being either better than or equivalent to the other algorithms in all tests conducted. By comparing the impulse response of SAA, BP, and FBP, Balla *et al.* found that BP and FBP performed similarly and better than SAA.[50] Using a dedicated breast CT image of an uncompressed patient breast, Van de Sompel *et al.* simulated a tomosynthesis acquisition and compared the reconstruction obtained with the FBP, SART, and MLEM.[51] As metrics, Van de Sompel *et al.* used the CNR and a numerical observer to estimate the area under the receiver operating characteristic (ROC) curve for detection of a lesion. Among other results mentioned in other sections of this review paper, Van de Sompel *et al.* performed a comprehensive analysis of the impact of the different reconstruction parameters relevant to each algorithm on the final image quality. The authors again confirmed that SART converges more quickly than

MLEM, while the noise amplification of MLEM is lower than that of SART. Overall, SART outperforms MLEM and FBP when tested with noiseless simulations, while MLEM obtains higher metrics in the simulations with noise present.

II.E. Reconstruction artifacts

Given the very limited sampling of the frequency domain involved in DBT acquisition due to the narrow angular range of the x-ray source motion, this imaging modality is very susceptible to artifacts of various kinds. Most common among these are the presence of shifted and repeated versions of high-contrast features located in adjacent planes. Various new methods and modifications to existing reconstruction algorithms have been proposed to reduce or eliminate this and other types of artifacts that appear commonly in DBT.

Wu *et al.* proposed an addition to the MLEM algorithm to reduce the presence of artifacts due to high contrast signals present outside the in-focus plane (Fig. 2).[52] In this algorithm, four methods of detecting which projections contain the appropriate information to contribute to the formation of each voxel were tested. The projections that are determined to contain "abnormal" information from out-of-plane artifacts are not used to update the reconstructed voxel. Of the four different "voting" methods investigated to achieve this identification, it was determined that their performance varies depending on the type of artifact present. The combination of two of these methods, the "projection segmentation" and "one-step classification" methods, results in an algorithm that can successfully remove artifacts due to both large and small calcifications. Ge *et al.* also proposed an algorithm to reduce the artifacts introduced by high contrast objects (large or dense microcalcifications, metal inserts) by estimating the shift variant impulse response of the system, applying it to the isolated object, and subtracting the resulting estimated artifact from the reconstruction.[53,54] Another method to remove artifacts due to calcifications was proposed by Erhard *et al.*, in which a hysteresis thresholding method is applied to the initial reconstruction to isolate the microcalcifications, which are then removed from the projections by interpolation and the results reconstructed.[55] Finally, the identified microcalcifications are added back into the reconstruction at their estimated locations. Sun *et al.* developed an algorithm to reduce the visibility of out-of-plane signals using a 3D nonlinear anisotropic diffusion filter that showed promising results.[56]

Zhang *et al.* proposed the use of a breast boundary detection method not only to remove the artifacts commonly seen in the periphery of the reconstructed breast, but also to increase the reconstruction speed (Fig. 3).[57] By performing breast boundary detection, the SART reconstruction can

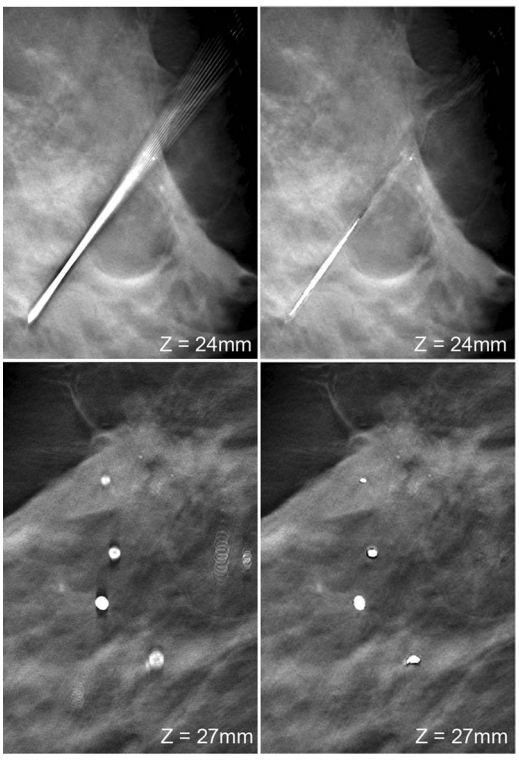

FIG. 2. Typical reconstruction artifacts found in DBT from out-of-plane high contrast objects (left) and the result of the correction proposed by Wu *et al.* (right). These examples show artifacts from a localization needle (top) and large microcalcifications (bottom). Reprinted with permission from Wu *et al.*, "Voting strategy for artifact reduction in digital breast tomosynthesis," Med. Phys. **33**(7), 2461–2471 (2006). Copyright © 2006, American Association of Physicists in Medicine.

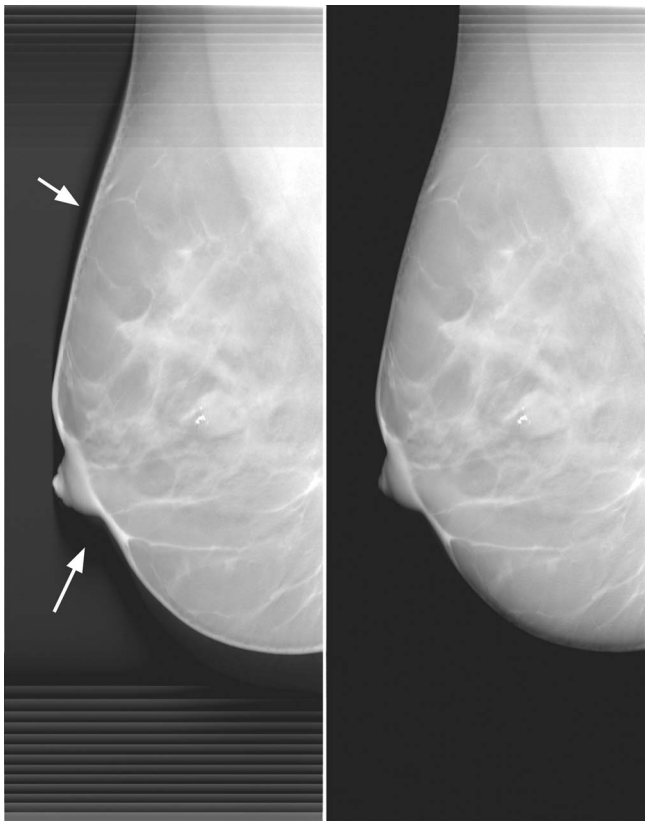

FIG. 3. Result of the correction proposed by Zhang *et al.* to remove the breast boundary artifacts (arrows) from DBT reconstructions. Reprinted with permission from Zhang *et al.*, "Application of boundary detection information in breast tomosynthesis reconstruction," Med. Phys. **34**(9), 3603–3613 (2007). Copyright © 2007, American Association of Physicists in Medicine (AAPM).

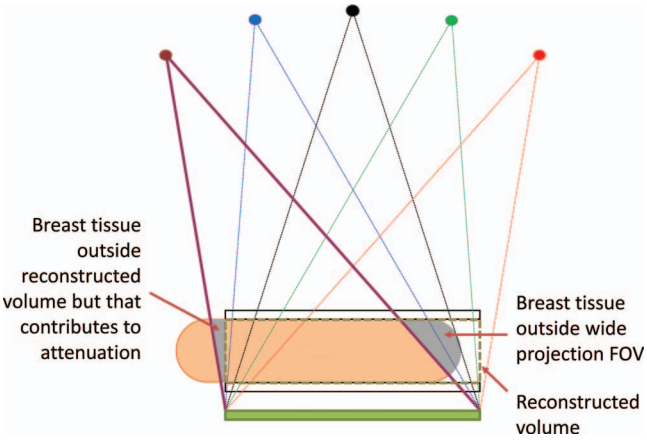

FIG. 4. Diagram of a typical DBT acquisition showing the source of two reconstruction artifacts. The gray areas show portions of the breast tissue that cause artifacts near the borders of the reconstructed volume (dashed box) in the x-ray tube motion direction. Examples of both of these artifacts can be seen at the top of the left image in Fig. 5; the bright area is due to the gray portion of breast tissue on the left of the diagram, while the horizontal stripes are due to the gray portion of breast tissue on the right.

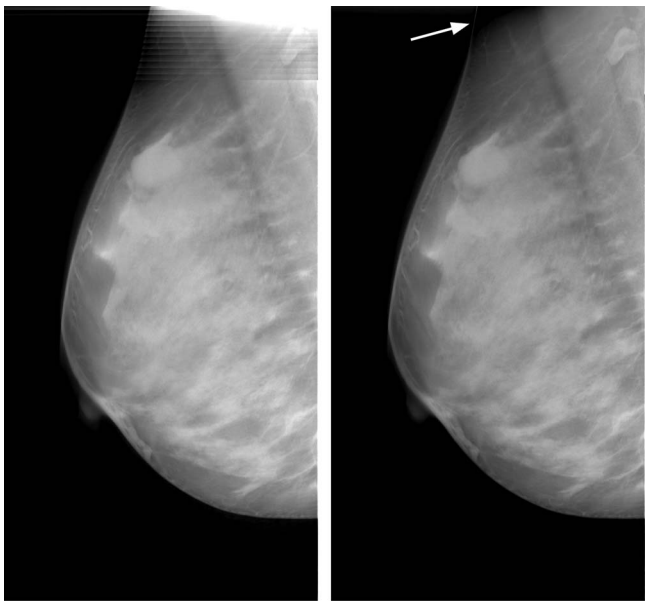

FIG. 5. Result of the algorithm proposed by Zhang *et al.* to reduce the detector boundary artifact commonly seen in DBT reconstructions. Reprinted with permission from Zhang *et al.*, "Artifact reduction methods for truncated projections in iterative breast tomosynthesis reconstruction," J. Comput. Assist. Tomogr. **33**(3), 426–435 (2009). Copyright © 2009, Lippincott Williams & Wilkins.

be performed only within the volume occupied by the breast, considerably decreasing the reconstruction time. In addition, the inclusion of only the volume occupied by the breast in the reconstruction allows for the removal of the artifact in the breast periphery, which appears due to the breast projection covering one area of the detector in some projection angles and not covering it for other projection angles.

Other common artifacts in DBT are truncation artifacts close to the detector edges due to the finite size of the detector and x-ray beam. The finite size of these items causes two different phenomena, described in Fig. 4, that result in bright horizontal lines and a bright area, as shown in Fig. 5 (left). Different algorithms have been proposed to correct these artifacts, showing promising results. To correct the horizontal line artifact due to wider projections not including portions of tissue (right gray area in Fig. 4), Li *et al.* proposed an algorithm for FBP,[58] actually tested on chest tomosynthesis images but relevant to DBT. In this algorithm, the number of rays that pass through each voxel in the volume being reconstructed is counted, resulting in a 3D "count map." This map is then used to weigh the corresponding intensities of the backprojected image. Zhang *et al.* corrected these artifacts when applied to SART reconstructions (Fig. 5).[59] To correct the same artifact as that addressed by Li *et al.*, the algorithm proposed by Zhang *et al.* updates the voxels in the reconstructed volume that are not covered by the projection being processed with the mean value of the neighboring region that is covered by the projection. To correct the artifact that appears as a bright area due to the tissue present outside the reconstructed field of view (left gray area in Fig. 4), Zhang *et al.* proposed to first detect which rays have traveled through tissue, rather than air, outside the reconstructed volume using a predetermined threshold. Upon identification of these rays, their contribution to the reconstruction is modified by assuming that the tissue outside the reconstructed volume consists of breast tissue with "average" attenuation. As can be seen in Fig. 5, the algorithms result of Zhang *et al.* in a correction of the artifacts, although in some cases the second algorithm over-compensates for the attenuation outside the reconstructed volume, resulting in a dark area in the final result [white arrow in Fig. 5 (right)]. In a recent follow up study, Lu *et al.* of the same group improved these correction methods and have been able to remove the dark area artifact in their processed images by refining the method used to estimate the path length traveled by the identified problematic rays within the breast tissue included in the reconstructed volume.[60]

II.F. Reconstructed slice thickness

Tomosynthesis reconstruction is normally performed to yield in-focus slices 1 mm apart or 1 mm thick slices. Which of these two theoretical descriptions is applicable depends on the reconstruction algorithm used. Diekmann *et al.* studied three different methods to combine ten 1 mm slices together to improve image quality mainly by reducing noise.[61] The algorithms tested in their work were: maximum intensity projection (MIP), simple averaging, and a novel algorithm called softMIP, which provides a weighted average of the pixels being combined. Using objective metrics, the authors found that MIP works best for microcalcifications, while averaging results in the best image quality for masses, with softMIP performing in between for both types of lesions. In addition to image quality improvement, merely reducing the number of slices that require interpretation while maintaining image quality would be a great contribution to DBT, given the concern for increased reading time of screening DBT images compared to mammography. Van de Sompel *et al.* also compared reconstructing thicker slices with SART and

ML with post-reconstruction binning of thin slices, although the method for this binning was not specified.[51] The authors found that post-reconstruction binning results in improved image quality compared to reconstructing thicker slices, with a maximum improvement being achieved at different thicknesses, depending on the reconstruction algorithm used. In this study, however, only masses were investigated, so the impact of binning on microcalcification visibility was not addressed.

II.G. Geometric calibration

Except for TACT-based reconstruction, all reconstruction algorithms rely on an accurate and complete understanding of the geometry used to acquire the projections to generate an optimal reconstructed volume. As determined by Mainprize *et al.*, of all the possible errors in acquisition geometry input, the only fixed error (same offset present in all projections) that affects image quality is detector yaw (relative angle between detector edge and x-ray source motion).[62] However, random variations of all kinds during the acquisition process result in both a loss of contrast and error in lesion localization.

To determine the geometrical parameters with ease and accuracy, Li *et al.* proposed to perform geometrical calibration using a phantom with a number of high contrast spherical markers with known locations.[63] From acquisition of projections of this phantom, matrix decomposition can yield the projection matrix that relates the volumetric locations to the projection locations. From this projection matrix, the x-ray source and central ray positions can be determined. In this work, Li *et al.* also showed the sensitivity of small detail to an accurate knowledge of the geometry, by introducing simulated errors in the geometric information and reconstructing a phantom with microcalcifications. In a follow-up study, Li *et al.* determined that, in practice, reconstruction errors due to sensitivity to the accuracy in the geometric calibration could be avoided by using many more markers than the minimum theoretically required (6), and by distributing them so that a large portion of the imaging volume is covered.[64]

III. IMAGE ANALYSIS AND PROCESSING

III.A. Synthetic mammograms

Currently, the single DBT system approved for clinical use in the U.S. by the Food and Drug Administration (FDA) is labeled for acquisition of a tomosynthesis image only combined with a mammographic image. Of course, this results in a radiation dose penalty of approximately double the dose of a single mammogram or tomosynthesis acquisition.[65] The need, correct or not, to always acquire a mammogram along with a DBT image results mainly from the suspicion that microcalcification detectability in DBT is inferior to that in mammography. Of the many studies comparing microcalcification detectability, some have found this inferiority,[66–68] while others have not.[69–73] To avoid this penalty, research is ongoing in creating a synthetic mammographic image from a tomosynthesis acquisition. In the only study on this matter, Gur *et al.* reported on an observer study to compare the performance of DBT combined with either an actual mammogram or a synthetic mammogram (Fig. 6).[74] With 114 cases and 10 readers, the authors found that combining the DBT image with the synthetic mammogram resulted in a loss of sensitivity with equivalent specificity. Therefore, the synthetic mammograms from tomosynthesis data used in that study were not capable of replacing actual mammographic acquisitions. However, the algorithms to synthesize these images are still being developed, and preliminary (unpublished) evaluations of more recent synthetic mammograms have shown substantial improvement.[75]

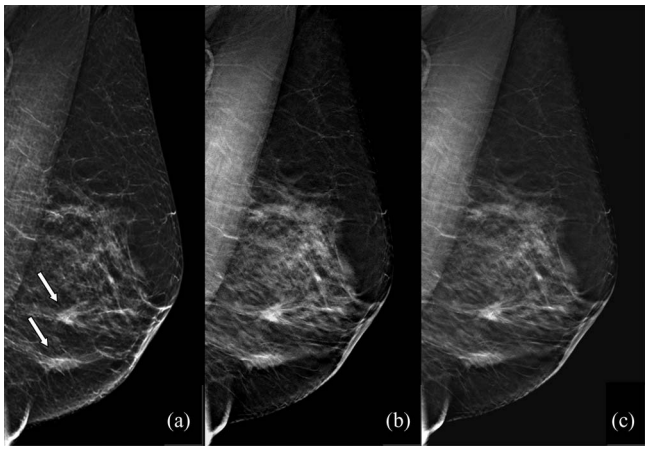

FIG. 6. (a) Digital mammogram (MLO view) of a patient showing two malignant masses, (b) synthetic mammogram constructed from the DBT data, (c) DBT slice. Reprinted with permission from Gur *et al.*, "Dose reduction in digital breast tomosynthesis (DBT) screening using synthetically reconstructed projection images: An observer performance study," Acad. Radiol. **19**(2), 166–171 (2012). Copyright © 2012, Association of University Radiologists (AUR).

III.B. Texture and glandular tissue analysis

Although not fully three-dimensional as dedicated breast CT images, DBT images do provide more information on breast tissue localization than mammography. The utility of this additional information for various tissue analysis aspects has been investigated. In two separate studies, Kontos *et al.* reported on the use of DBT images to determine any correlations between parenchymal texture features and breast glandular areal density or risk estimates.[76,77] In the initial study, Kontos *et al.* first analyzed the correlation between several texture feature metrics (skewness, coarseness, contrast, energy, homogeneity, and fractal dimension) from DBT and mammography images to the Gail and Claus risk models, finding overall low correlation.[76] However, a significant correlation was found between some of the texture feature metrics and glandular density, both with mammography and DBT, with the latter resulting in stronger correlations. This finding was repeated in the follow-up study with a larger number of patient cases.[77] It seems that being able to perform the analysis of the parenchymal texture without the effect of overlapping tissue present in mammograms could provide more

reliable information on characteristics that may be related to breast cancer development risk. It should be noted, however, that in another study Kontos *et al.* found that the values of different feature metrics may vary with acquisition parameters (angular range, number of projections). So although this allows for optimization of acquisition parameters for this type of texture analysis, it also means that care should be taken to note the source of images used for feature analysis and inter-image comparisons.[78]

Engstrom *et al.* studied tomosynthesis projections and reconstructions of 55 patient breasts to determine the power law coefficient (β in the equation $PS(f) = k/f^{\beta}$) associated with the power spectrum of normal breast tissue background.[79] In this study, the authors found that β for the tomosynthesis projections had a mean of 3.06, while for the reconstructions the value of β was 2.87, with the difference being statistically significant. In a more recent study, Chen *et al.* found that the mean values of β of 23 patients in dedicated breast CT, DBT, and mammography images were 1.75–1.83 (3 orthogonal views in breast CT), 3.06–3.10 (CC and MLO in DBT), and 3.17–3.30 (CC and MLO in mammography).[80] Although small, the difference in β between tomosynthesis and mammography was statistically significant for all comparisons but one (MLO from tomosynthesis and CC from mammography). Hu *et al.*, however, found that the values of β for the tomosynthesis reconstructions could vary substantially depending on the filters used during FBP reconstruction.[81] In previous studies, a smaller value of β has been related to improved mass detectability.[82]

Bakic *et al.* compared the breast glandular areal density estimation from mammograms and the central (0°) tomosynthesis projections using previously validated semi-automated density estimation software.[83] Although the acquisition geometry of these two images is essentially equal, two major differences negatively impact the image quality of the central tomosynthesis projection compared to the corresponding mammogram. In the first place, the tomosynthesis projection will be considerably noisier, given that the exposure used to acquire it is only a fraction (in this case an average of 22%) of that used for mammogram acquisition. In addition, the overall contrast can be expected to be lower, since currently DBT is acquired without an x-ray scatter grid, and therefore the full impact of the scatter signal on the image contrast is included in the tomosynthesis projection. To perform this comparison, three experienced independent readers used a density estimation software (CUMULUS, version 4.0; University of Toronto, Toronto, Canada)[84] involving several manual steps. Each reader obtained a glandular density estimate from all 39 cases twice, with each repeated analysis separated by 2 months. Although the density estimation results obtained by Bakic *et al.* between the mammography images and tomosynthesis projection images were highly correlated ($\rho = 0.91$), the latter-based estimations were slightly but significantly higher.[83] In addition, the intrareader correlations were slightly, but not significantly, higher for the mammogram-based analysis.

Tagliafico *et al.* compared the density estimation from mammograms to the average of the estimation of all 15 tomosynthesis projection images acquired in 50 patients.[85] Using two different methods, the authors found that the density estimation from mammograms was significantly higher than from tomosynthesis projections. Given that no independent truth is available, it is unclear if mammography overestimated or tomosynthesis underestimated the density. In another study, Bakic *et al.* compared the mammographic density estimation to the 3D density estimation from DBT using a semiautomated thresholding technique and found moderate agreement.[86] They also found that, on average, DBT results in lower density estimates than mammography.

Although several classification algorithms to identify the different breast tissues present in dedicated breast CT images have been developed,[87–91] classification based on DBT images was first proposed by Kontos *et al.*[92] and a method completely developed by Vedantham *et al.*[93] Kontos *et al.* investigated the use of different texture features (e.g., skewness, coarseness, etc.) to identify regions in DBT reconstructions as dense or fatty. The authors hypothesized that image classification could be achieved using this type of region-based analysis. To test the feasibility of their approach, Kontos *et al.* performed ROC analysis on the ability of these different metrics to differentiate between the two tissue types, finding that for DBT reconstructions the fractal dimension results in the highest area under the ROC curve. Vedantham *et al.* on the other hand used a fuzzy c-means based segmentation method, among other processing steps, to perform the tissue classification.[93] The method proposed by the authors is capable of classifying breast skin, adipose, and glandular tissues, in addition to muscle and, with some input from the user, suspicious lesions. Such a classification method could be useful for reconstruction, computer aided detection (CADe), breast glandular volumetric density, and registration, which may be useful for comparison of current acquisitions with priors.

III.C. Image evaluation with numerical observers

The use of numerical observers in medical imaging research is advantageous since it allows for comparison of image quality for specific tasks which include a very high number of cases and/or imaging parameters without undergoing costly or unfeasible human observer studies. However, for tomosynthesis research, the use of numerical observers is currently challenging due to a lack of models that incorporate the additional pseudo-3D information provided in this imaging modality. As an example of this limitation, some optimization studies, some of which have been mentioned above, have used 2D numerical observers to analyze only the slice that crosses the center of the signal of interest. Although this may be the case, it has not been shown that optimization based on this single tomosynthesis slice perfectly correlates with one based on the entire or portion of the reconstructed volume. It could be expected that for lesions that span more than a single slice, the quality of the representation of that lesion throughout the entire lesion volume does not necessarily correlate perfectly with the quality of the lesion presentation of the center slice. Young *et al.* proposed to use a numerical observer model to analyze the tomosynthesis projections, not the

reconstructions, incorporating into the model the spatial correlations present due to acquisition of the same volume from different projection angles.[94] The authors showed that the results of the observer model analysis of the projections are different if these spatial correlations are taken into account. By performing the analysis on the projection space rather than the reconstruction space, the authors suggest that the results obtained provide an upper-bound on the performance results, without introducing additional variability from the reconstruction algorithm methods and parameters. Park *et al.* proposed a 3D ideal observer model that can be applied to tomosynthesis reconstructed images to analyze lesion detectability.[95] A study comparing the 3D observer model to the 2D model, applied both to the slice including the lesion and in projection space, would be of great interest.

Gang *et al.* derived a 2D detectability index from a 3D cascaded systems analysis and compared its predictions to human observer performance for lesion detection with varying acquisition parameters.[96] The authors found reasonable correspondence between model predictions and observer performance, allowing for the use of their developed model for optimization in 3D imaging such as DBT.

III.D. Computer aided detection of masses

The use of CADe in digital mammography has become common practice in the clinical realm. It could be expected that similar systems, if available, would be adopted for DBT, especially considering the larger amount of data presented to the reader in a DBT image compared to a mammogram. In an early study, Reiser *et al.* proposed a CADe method for mass detection based on detection and segmentation of suspicious lesions using a radial gradient index method.[97] Inclusion of the vertical direction information did not improve classification performance based on gradient analysis, but it did improve performance based on shape analysis. Overall, the sensitivity for the proposed algorithm was 76% with 11 false positives per exam. In another early study, Chan *et al.* also proposed a CADe method for mass detection, which they tested on 26 patient DBT cases.[98] The method, which involved interpolation of the reconstructed image to obtain cubic voxels with 0.1 mm sides, gradient field analysis to identify candidate lesions, segmentation via 3D region growing, and feature analysis, resulted in an 85% sensitivity with 2.2 false positives per exam and 80% sensitivity with 2.0 false positives per exam, depending on the operating point setting. In a follow-up study, Chan *et al.* investigated how the performance of this algorithm was affected by the number of projection views and the dose level used to acquire the DBT image.[99] For this, they analyzed a set of patient images reconstructed by using either all 21 projections acquired or only 11 of the 21 projections (which resulted in about half the radiation dose). Although the performance of the classifier was unaffected by the lower number of projections and dose, the overall area under the ROC curve was lower for the 11 projection images, due to an increase in the false positive rate.

In a different approach, Reiser *et al.* proposed to perform automated mass detection by analyzing the acquired tomosynthesis projection images as opposed to the reconstructed images.[100] By using the projections, the authors argue that any artifacts introduced by the reconstruction algorithm are avoided. In their method, only an intermediate step involves analysis in reconstruction space, in which the algorithm attempts to identify and eliminate the suspicious lesions due to tissue superposition. The initial lesion identification and final lesion classification is performed in projection space. With their limited data set, the authors found a sensitivity of 90% with 1.5 false positives per exam. Chan *et al.* later compared the performance of CADe for mass detection under three conditions: when the algorithm performs all analysis on the reconstructed images only, when the algorithm performs the lesion identification and classification on the projection images and then applies a decision threshold on the distribution of mass likelihood scores obtained from the projections and backprojected to reconstruction space, or, finally, when the algorithm combines the likelihood scores of both methods described above to arrive at a final decision.[101] The authors found that taking advantage of the most information available, i.e., using the approach that combines the 2D and 3D-based results, yields the highest performance, with a false positive rate of 1.23 and 2.04 per exam at sensitivities of 80% and 90%, respectively. Singh *et al.* also proposed to perform the initial lesion identification in projection space with the rest of the algorithm performed in reconstruction space.[102] As opposed to the previous algorithms proposed, however, the lesion classification performed by Singh *et al.* was not feature-based, but used information theory-based analysis with mutual information as the metric of choice and three different ways of constructing a knowledge base for training of the system. The authors found that although there was no statistically significant difference in the performance of the system when trained by either of the three knowledge bases, the inclusion in the knowledge base of true and false positive regions of interest (ROI), identified by the first stage of the CADe process, yielded the highest area under the ROC curve. However, the authors argue that a knowledge base consisting of only true positive and normal ROI may be more robust and generalizable, since it does not depend on the performance and characteristics of the first stage of the system. In a subsequent study, Mazurowski *et al.* demonstrated that a mutual information based algorithm, trained solely with mammographic images, can perform comparably in detecting masses in DBT images, with a simple preprocessing of the DBT reconstructions in which an area close to the breast edge is masked out.[103]

III.E. Computer aided diagnosis of masses

A computer aided diagnosis (CADx) system for characterization of suspicious masses was developed and tested by Chan *et al.* on both the tomosynthesis reconstructions and the projections.[104] After a ROI was marked by the reader in a reconstructed slice, the location of the ROI in the acquired projections was identified, and the same CADx algorithm with few modifications processed both image spaces independently. The authors found that reconstruction-based performance is significantly higher than projection-based

performance, with the area under the ROC curve as the figure of merit.

III.F. Computer aided detection and diagnosis of microcalcifications

For automated detection of microcalcification clusters, in an early preliminary study, Peters *et al.* proposed to use wavelet filtering and fuzzy processing of the acquired projections to avoid performance variations due to different reconstruction algorithms and parameters.[105] Reiser *et al.* also proposed a method that performs the initial suspicious lesion identification and final feature-based classification in projection space, while using reconstruction space in an intermediate step to eliminate suspicious areas that appear in few projections.[106] In this preliminary study with a limited data set, the authors obtained a sensitivity of 86% with 1.3 false positives per exam, yielding a poorer performance than current digital mammography CADe algorithms for microcalcifications. In another study, Park *et al.* studied the use of a modified version of an existing CADe algorithm for microcalcification detection in mammography in DBT.[107] For this, the authors added a clustering method to the existing algorithm to determine if the calcifications identified in the acquired projections (when the algorithm was applied to projection space) or reconstructed slices (when applied to reconstruction space) belong to the same cluster. Upon identification of the potential clusters, four different methods to arrive at the final identification were compared. The authors found that the best method for projection based analysis yielded a sensitivity of 70% with 4.0 false positives per exam, while the reconstruction based analysis resulted in 88% sensitivity with a 15.9 false positive rate. Using a reconstruction based CADe method for microcalcifications derived from an algorithm for mammography, Bernard *et al.* obtained promising results, with a sensitivity of 85% with 1.4 false positives per exam.[108] The authors note that this performance level is lower than that obtained with the similar algorithm used for mammography (86% sensitivity with 0.95 false positives per exam), again demonstrating that further work is required for tomosynthesis-based CADe to match the performance in mammography in identifying microcalcifications. Sahiner *et al.*, using an algorithm that processes only the reconstructed images, obtained a sensitivity for microcalcification detection of 85% with 3.8 false positives per exam in an abnormal case set and with 3.4 false positives per exam in a normal case set.[109] Finally, in early work, Ho *et al.* have proposed CADe and CADx of microcalcifications for DBT using epipolar curves.[110–112]

III.G. Image registration

Several clinical applications for registration of DBT images have been identified and methods for each are being investigated. In the first place, comparison of DBT acquisitions with mammographic priors will be required if DBT replaces mammography as a screening technology. For this, as initial first steps, Bakic *et al.* performed registration of mammograms with the central (0°) tomosynthesis projection[113] and with a set of tomosynthesis projections,[114] using a previously described non-rigid registration algorithm, resulting in a correction of $\geq$90% of the per pixel intensity differences originally existing between the image pairs.

Van Schie *et al.* have proposed that when interpreting two views of the same breast during DBT screening, either by a human reader or a CAD system, there will be a need to determine corresponding locations in the two views.[115] For this, the authors proposed a model in which the breast, compressed for acquisition of the first view, is decompressed, rotated, and re-compressed for acquisition of the second view. By characterizing the translation of locations with this model, the authors developed an analytical solution for the transformation, yielding a fast method to perform this location matching. Using two-view patient cases in which different features were located by hand in each view, the method developed was tested and found to yield a median 3D distance between the actual and predicted location of 14.6 mm, with about half of the predictions being one or fewer slices away from the truth. Zhang *et al.*, in an initial study, developed an automated method to detect corresponding feature locations in two tomosynthesis projection images, which allowed for subsequent non-rigid registration.[116] Although the authors tested only registration of projection pairs from acquisition of contra-lateral breasts or from different projection angles of the same breast, the application of the same method for temporal registration would be possible. Since Sihna *et al.* successfully tested the registration of two DBT images acquired at separate time points by manually identifying matching feature locations,[117] it seems that incorporating the feature selection process using an algorithm like that proposed by Zhang *et al.* could result in a successful fully automated temporal registration method.

In a different approach to the registration of two DBT acquisitions separated temporally, Yang *et al.* proposed to perform the registration of the two volumes during their reconstruction from the acquired projections, using an iterative approach in which the optimization of the registration transformation between the two volumes is also included in each iteration step.[118] Using simulated data from a phantom and from a patient breast MRI acquisition, the authors found improved reconstruction and registration performance when the two tasks are performed combined rather than sequentially.

III.H. Quantitative breast tomosynthesis

Due to its very limited angular sampling, it is not apparent that DBT can provide quantitative information on the tissues present in the imaged volume. To investigate the feasibility of quantitative analysis in DBT, Shafer *et al.* used simulated and physical phantoms with varying layers of tissues and signals with a range of fractions of adipose and glandular tissue mixtures.[119] Their investigation involved the application of a background uniformity correction to the acquired images and analyzed how the presence of scatter, variation in background tissue composition, lesion vertical location, and x-ray spectrum used for acquisition impacted the estimated glandular density of the inserts. The authors found promising results for the quantitative potential of

tomosynthesis, but the use of overall homogeneous phantoms limits the generalizability of the results, calling for further investigation with more realistic breast phantoms and clinical cases. Richard and Samei developed a model to predict estimation task performance based on frequency based analysis, similar to the detectability analysis commonly used to predict signal visibility, but for tasks involving quantitative analysis, e.g., area and volume estimation.[120,121] This model was used to determine the optimal geometrical acquisition parameters that would maximize the precision of area and volume estimation in DBT reconstructions.

IV. ADVANCED APPLICATIONS

IV.A. Contrast enhanced breast tomosynthesis

As with contrast enhanced digital mammography, DBT imaging with iodinated contrast enhancement aims to interrogate the vascular characteristics of the imaged breast to improve malignant lesion detectability. Contrast-enhanced image characteristics that could help detect and diagnose malignant breast lesions include degree of enhancement, location of enhancement, and, with multi-acquisition dynamic protocols, enhancement kinetics.[122] Given the high in-plane spatial resolution and short acquisition time of DBT compared to dynamic contrast-enhanced breast magnetic resonance imaging (DCE-MRI), it seems that this imaging modality could prove useful in determining enhancement details in terms of both location and time. However, acquisition of enhancement kinetic curves with a high number of time points is a potential limitation for contrast-enhanced DBT (CE-DBT) given the use of ionizing radiation during acquisition. This results in an upper limit of probably three or four time points that can be used for constructing a kinetic curve, even with the most advanced CE-DBT technologies discussed below. In contrast, with DCE-MRI, acquisition of more than ten time points for kinetic curve analysis has been recently reported.[123,124] However, the need for more than a few time points to construct a kinetic curve is still being investigated.[125] Therefore, given the high spatial resolution and the high temporal resolution (although with few time points) achievable, CE-DBT has been studied extensively. If the limited number of acquisition time points possible with this imaging modality is a true limitation is a clinical question that seems yet to be answered.

IV.B. Contrast enhanced breast tomosynthesis: Temporal subtraction

Carton *et al.* were the first to propose performing CE-DBT.[126] In their approach, they used temporal subtraction, in which acquisition is performed before and after injection of the contrast agent, and the resulting reconstructions subtracted from each other. Using empirical data and theoretical modeling, the authors investigated the quantification of iodine concentration and the impact of the presence of x-ray scatter, patient motion, and detector stability. For this, the x-ray spectrum had to be modified to increase the fluence of x-rays above the K-shell of iodine (33.2 keV). Therefore, the authors used a tube voltage of 49 kVp and an added copper filter 0.27 mm thick, resulting in a first HVL of 3.06 mm Al. The authors found that the concentration of iodine could be underestimated due to scatter by 28%–54% for breast thicknesses ranging from 20 to 80 mm, respectively, while detector instability could introduce up to an 8% error in quantification. Patient motion between image acquisitions could result in an additional error depending on the amount of displacement and the iodine concentration in the location of interest. Finally, as expected, patient motion also results in subtraction artifacts visible in the resultant iodine only image. In another study on temporal CE-DBT, Chen *et al.* imaged 13 patients, of which 11 had malignancies proven by pathology, using light breast compression so as to not affect the flow of blood (and contrast agent) in the breast.[127] The authors found that CE-DBT resulted in enhancement of suspicious lesions in 10 of the 11 malignancies and no enhancement in the remaining two benign cases.

IV.C. Contrast enhanced breast tomosynthesis: Dual energy

To minimize patient motion issues, Carton *et al.* suggested the use of dual energy subtraction, in which both acquisitions are performed post-contrast injection, with one acquisition using an x-ray spectrum with most or all x-rays below the iodine K-shell energy and the other acquisition with an x-ray spectrum with most or all x-rays above this shell energy, rather than temporal subtraction.[126] Subsequent investigations on CE-DBT used this approach. Glick and Didier simulated the acquisition of the high and low energy images of a structured breast phantom using the x-ray spectra produced by a tungsten target with a tube voltage of 60 kVp, filtered with 0.4 mm of cerium, and 0.6 mm of tin, respectively.[128] The computer simulations showed that the lowest iodine concentration tested, 1.0 mg I/cm^3, could be seen in the subtracted image. In another study Puong *et al.* also proposed dual energy CE-DBT, but, as opposed to Glick and Didier who first reconstructed the low and high energy images and then performed weighted subtraction, this study proposed to first combine the acquired projections to obtain an iodine only projection set using a novel algorithm developed for contrast enhanced mammography,[129] and then reconstruct using the SART algorithm.[130] In addition to showing feasibility, Puong *et al.* performed an optimization of the x-ray spectra to be used for acquisition, and studied the effect of x-ray scatter on the quantification of iodine. In a subsequent optimization study, Puong *et al.* compared the image quality obtained using different target/filter combinations, and found that a Rh/Rh target/filter combination spectrum with a tube voltage of 27 kVp and a Mo/Cu spectrum with 49 kVp and a 0.48:0.52 dose ratio, respectively, results in the lowest image noise.[131] In addition, the authors proposed corrections for the quantification of iodine in the presence of scatter, nonconstant breast thickness at the breast borders, and limited vertical resolution. Later on, this same research group introduced a regularization to the SART reconstruction specific to iodine only reconstructions, showing improved image quality.[132]

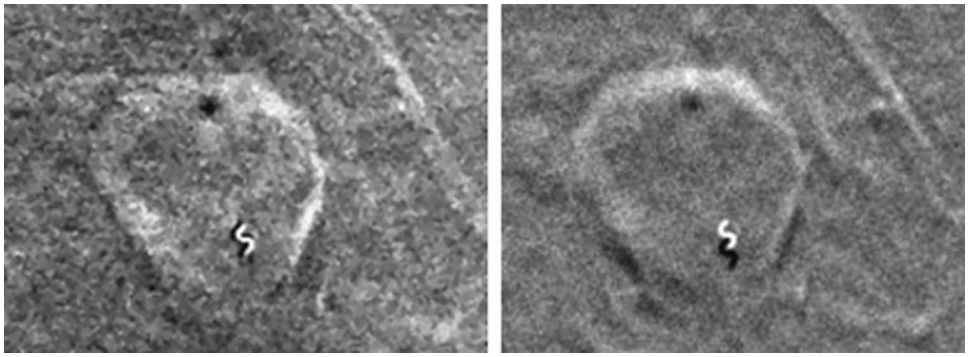

FIG. 7. ROI of a contrast enhanced DBT reconstruction of a patient with a malignant mass. (Left) Dual energy subtraction; (right) temporal subtraction. The presence of motion in the temporal subtraction is apparent. Reprinted with permission from Carton *et al.*, "Dual-energy contrast-enhanced digital breast tomosynthesis: A feasibility study," Br. J. Radiol. **83**(988), 344–350 (2010). Copyright © 2010, The British Institute of Radiology.

In the first dual energy studies involving patients, Carton *et al.* imaged patients with suspicious findings using both temporal subtraction and dual energy subtraction.[133,134] For this, after one pre-contrast injection acquisition to perform temporal subtraction with a high energy spectrum (49 kVp, 25 μm Rh + 0.25 mm Cu, 3.36 mm Al HVL), the authors acquired two sets of two images post-injection, each with a low energy spectrum (30 kVp, 25 μm Rh, 0.44 mm Al HVL) and the high energy spectrum. The dual energy approach resulted in less motion artifacts than the temporal subtraction (Fig. 7), which is an expected benefit of the former, but the authors proposed that with adequate motion correction, temporal subtraction may ultimately result in better image quality due to better background subtraction and lower noise. The same research group developed and validated a theoretical model to optimize the acquisition parameters to be used for dual energy CE-DBT with a photon counting, scanning multi-slit imaging system.[135,136] In this study, the authors aimed to perform acquisition of the low and high energy images simultaneously by selectively filtering the x-ray beam incident on adjacent detector slits. This necessitates the use of the same tube target, voltage, and current-exposure time product for both images, allowing only for a change in the beam filtration. Therefore, the authors investigated the optimization of the thicknesses of the two filter materials (tin for the low energy beam and copper for the high energy beam), the number of slits covered by each of the filter materials, and the weight factor w_t that is used in the equation to obtain the enhancement-only subtracted image:

$$I_{DE} = \ln(I_{Cu}) - w_t \ln(I_{Sn}) \text{ from Ref. 134,} \quad (1)$$

where I_{DE}, I_{Cu}, I_{Sn} are the subtraction, high energy copper-filtered and low energy tin-filtered images, respectively. As the figure of merit, Carton *et al.* used the signal difference to noise ratio (SDNR) normalized by the square root of the mean glandular dose, a common metric for this type of optimization study. The investigators found that a 2:1 copper and tin slit assignment is optimal, which can be translated in other system designs to assigning 2/3 of the available total exposure to the high energy image, combined with 0.16 mm tin and 0.23 mm copper filters. For this setup, the optimal weight factor varies with breast thickness and the breast tissue glandular fraction aimed to be suppressed. Of course, using a different weight factor for each breast thickness is not challenging, but it is for varying glandular fraction pairs. Overall, the authors found that a weight fraction of between 0.52 and 0.60, depending on the breast thickness, is optimal. Although the system this optimization model was based on is not being further developed, the methods and results of this investigation are still relevant for dual energy CE-DBT performed with other system designs. In a recent optimization study, Samei and Saunders also investigated the optimal weight factor, exposure distribution between the two images, and the x-ray spectra shape, using computer simulated acquisitions of a breast phantom.[137] One important distinction between this work and the work of Carton *et al.* was that the latter performed the logarithmic subtraction of the reconstructed images, while Samei and Saunders found that for their setup this method introduces artifacts, which are avoided if the subtraction is performed on the projections and the result used for reconstruction. Although Samei and Saunders investigated the use of different tube voltages for the two images, they found that a tube voltage of 49 kVp is optimal for both acquisitions, a very important simplification of the required hardware. In terms of filtration, the optimal thicknesses were found to be 92.5 μm of copper and 95 μm of tin for the high and low energy acquisitions, respectively. For this combination of filters, the optimal weight factor and dose distribution is 0.61 and 0.54 (high energy image dose to total dose fraction), respectively.

In a different approach to dual energy acquisition taking advantage of new technology, Schmitzberger *et al.* reported on a study that used an energy discriminating photon counting multi-slit tomosynthesis system.[138] The detector used in this system can discriminate between detected x-rays with energy below and above a certain threshold.[139] Of course, for iodinated contrast-enhanced imaging, the threshold is set at the K-shell energy of iodine, and therefore a single DBT acquisition can be performed that still results in a low energy and a high energy image. This guarantees perfect tissue registration, so no subtraction artifacts due to patient motion are possible, and it can result in lower total glandular dose per exam. In this study, the glandular dose delivered per acquisition was 0.42 mGy, and three acquisitions at three different time points were performed for each patient to obtain dynamic

data. In phantom imaging with a contrast agent concentration of 3 mg I/cm^3, the smallest simulated lesion that could be detected was 5 mm diameter (the next smallest lesions present were 1 and 2 mm diameter). The preliminary patient study included in this work showed promising results.

In a study on how contrast dynamics and acquisition timing affect iodine quantification, Hill *et al.* found that the tomosynthesis-based results will reflect the average concentration during acquisition, but that a correction factor for different lesion sizes is needed to obtain accurate quantification results.[140] In addition, the same research group found that the most accurate quantitative assessment is obtained when both the low and high energy projections are acquired in a single x-ray source sweep with fast tube voltage switching.[141]

IV.D. Multimodality imaging

The combination of several imaging technologies with DBT has been investigated. Given that DBT as stand-alone technology has only recently been introduced to the clinical realm, it is not surprising that multimodality approaches are still at a very infant stage. One research group has investigated the combination of DBT with electrical impedance tomography for characterization of suspicious lesions, showing promising results with a small number of patient cases.[142–144] Combining DBT with ultrasound has also been investigated, with the development of a prototype system that acquires the tomosynthesis image and immediately afterwards positions and scans an ultrasound probe across the compressed breast, obtaining a co-registered 3D ultrasound image.[145,146] The combination of morphological information with functional information is also being developed by a group that is investigating combining DBT with limited angle Tc-99m sestamibi-based single photon emission computed tomography (SPECT).[147–149] The preliminary patient study performed showed that adding the functional information can improve the performance of DBT, especially in improving specificity.[149] Finally, DBT combined with diffuse optical tomography for interrogation of the hemoglobin and oxygen saturation state has been also investigated, with the optical characteristics of malignant lesions having been found to be different than benign lesions and normal tissues.[150–152] Therefore, it seems that diffuse optical tomography could provide useful additional information to help characterize lesions with DBT.

IV.E. Phase contrast tomosynthesis

Phase contrast imaging has been investigated for various modalities due to its potential to improve contrast and enhance feature edges.[153–155] Given the promising results for applications such as radiography, mammography and CT, the possibility of performing phase contrast DBT is intriguing. Using a benchtop system, Hammonds *et al.* developed and tested the combination of phase contrast radiography with tomosynthesis imaging on phantoms.[156] In their study, the authors determined that this edge enhancement is retained during tomosynthesis reconstruction, therefore making phase contrast DBT feasible and promising.

IV.F. Tomosynthesis elastography

From ultrasound imaging, it is known that benign and malignant breast lesions exhibit differences in their elasticity. To assess elasticity or differences in elasticity, one theoretically simple method especially applicable to DBT could be to measure strain, in this case defined as the change in lesion size in one direction under varying levels of compression force. To investigate this potential new application for DBT, Kim *et al.*[157] and Engelken *et al.*[158] proposed to perform elastography using a DBT system by acquiring subsequent images of the breast undergoing different amounts of mechanical breast compression. In the preliminary phantom study using DBT performed by Engelken *et al.*, promising results were obtained.[158]

IV.G. Therapy

In image-guided radiation therapy, patient positioning pre-irradiation is of utmost importance to ensure accurate dose delivery to the tumor and sparing of the healthy tissue. The introduction of on-board cone-beam CT (CBCT) allowed for 3D verification of patient positioning, but raised concerns of the dose involved during imaging, in addition to extended image scan time and gantry rotation issues. To address these limitations, on-board tomosynthesis imaging using the kV source and planar detector used for CBCT has been proposed. Of course, compared to on-board radiography, tomosynthesis provides improved soft tissue contrast and partial information in the third dimension, while reducing the dose, acquisition time, and gantry travel involved in on-board CBCT. As with the diagnostic imaging application, the research performed on DBT for therapy has focused on optimizing the acquisition geometry[159–163] and characterizing the radiation dose involved,[160,164] in addition to therapy-specific issues, such as comparison to reference images[165] and localization of surgical clips.

V. CONCLUSIONS

The breast tomosynthesis process does not end with acquisition of the projection images. In addition to the obvious importance of the reconstruction process, many algorithms may be used to further improve the resulting images and to extract additional information from them. Due to the infancy of DBT in the clinical realm, some of these additional processes and analyses have had a limited chance of being tested in large clinical patient data sets, hampering our ability to gauge their true performance. Future research will surely involve the testing of these algorithms on larger clinical data sets for further characterization and optimization of their performance. In parallel, the introduction of DBT to the clinic will continue to motivate the development of advanced versions and applications of this imaging technology in addition to its combined

use with other modalities that can provide functional and/or physiological information of the breast.

ACKNOWLEDGMENTS

The work by our group discussed here has been supported by the Atlanta Clinical and Translational Science Institute, the University Research Committee of Emory University, the National Science Foundation (DMS-1115627), the National Cancer Institute (R01CA163746, P50CA128301), and the National Center for Research Resources (UL1RR025008). The content is solely the responsibility of the author and does not necessarily represent the official views of these institutions. The author would like to thank Dr. Wei Zhao, Dr. Tao Wu, Dr. Heang-Ping Chan, Dr. David Gur, Dr. Ann-Katherine Carton, and Dr. Andrew Maidment for giving permission to reprint their figures, Dr. James Nagy and Steve Feng for scientific input and Jessica Paulishen for assistance with editing.

[a]Author to whom correspondence should be addressed. Electronic mail: isechop@emory.edu; Telephone: (404)712-2412; Fax: (404)712-5813.

[1]J. T. Dobbins III and D. J. Godfrey, "Digital x-ray tomosynthesis: Current state of the art and clinical potential," Phys. Med. Biol. **48**, R65–R106 (2003).

[2]T. Mertelmeier, J. Orman, W. Haerer, and M. K. Dudam, "Optimizing filtered backprojection reconstruction for a breast tomosynthesis prototype device," Proc. SPIE **6142**, 61420F (2006).

[3]B. Zhao and W. Zhao, "Three-dimensional linear system analysis for breast tomosynthesis," Med. Phys. **35**, 5219–5232 (2008).

[4]B. Zhao, J. Zhou, Y.-H. Hu, T. Mertelmeier, J. Ludwig, and W. Zhao, "Experimental validation of a three-dimensional linear system model for breast tomosynthesis," Med. Phys. **36**, 240–251 (2009).

[5]X. Wang, J. Mainprize, G. Wu, and M. Yaffe, "Task-based evaluation of image quality of filtered back projection for breast tomosynthesis," in *Proceedings of the 10th International Workshop on Digital Mammography* (Springer Berlin Heidelberg, Girona, Spain, 2010), pp. 106–113.

[6]T. Mertelmeier, J. Ludwig, B. Zhao, and W. Zhao, "Optimization of tomosynthesis acquisition parameters: Angular range and number of projections," in *Proceedings of the 9th International Workshop on Digital Mammography* (Springer Berlin Heidelberg, Tucson, AZ, 2008), p. 220–227.

[7]J. Orman, T. Mertelmeier, and W. Haerer, "Adaptation of image quality using various filter setups in the filtered backprojection approach for digital breast tomosynthesis," in *Proceedings of the 8th International Workshop on Digital Mammography* (Springer Berlin Heidelberg, Manchester, 2006), pp. 175–182.

[8]J. Zhou, B. Zhao, and W. Zhao, "A computer simulation platform for the optimization of a breast tomosynthesis system," Med. Phys. **34**, 1098–1109 (2007).

[9]G. T. Herman and A. Lent, "Iterative reconstruction algorithms," Comput. Biol. Med. **6**, 273–294 (1976).

[10]J. Ludwig, T. Mertelmeier, H. Kunze, and W. Härer, "A novel approach for filtered backprojection in tomosynthesis based on filter kernels determined by iterative reconstruction techniques," in *Proceedings of the 9th International Workshop on Digital Mammography* (Springer Berlin Heidelberg, Tucson, AZ, 2008), pp. 612–620.

[11]Y. Chen, J. Y. Lo, and J. T. Dobbins III, "Importance of point-by-point back projection correction for isocentric motion in digital breast tomosynthesis: Relevance to morphology of structures such as microcalcifications," Med. Phys. **34**, 3885–3892 (2007).

[12]B. Claus, J. Eberhard, A. Schmitz, P. Carson, M. Goodsitt and H.-P. Chan, "Generalized filtered back-projection reconstruction in breast tomosynthesis," in *Proceedings of the 8th International Workshop on Digital Mammography* (Springer Berlin Heidelberg, Manchester, 2006), pp. 167–174.

[13]R. Gordon, R. Bender, and G. T. Herman, "Algebraic reconstruction techniques (ART) for three-dimensional electron microscopy and x-ray photography," J. Theor. Biol. **29**, 471–481 (1970).

[14]P. Gilbert, "Iterative methods for the three-dimensional reconstruction of an object from projections," J. Theor. Biol. **36**, 105–117 (1972).

[15]A. H. Andersen and A. C. Kak, "Simultaneous algebraic reconstruction technique (SART): A superior implementation of the ART algorithm," Ultrason. Imaging **6**, 81–94 (1984).

[16]Y. Zhang, H.-P. Chan, B. Sahiner, J. Wei, M. M. Goodsitt, L. M. Hadjiiski, J. Ge, and C. Zhou, "Tomosynthesis reconstruction using the simultaneous algebraic reconstruction technique (SART) on breast phantom data," Proc. SPIE **6142**, 614249 (2006).

[17]Y. Lu, H.-P. Chan, J. Wei, and L. M. Hadjiiski, "Selective-diffusion regularization for enhancement of microcalcifications in digital breast tomosynthesis reconstruction," Med. Phys. **37**, 6003–6014 (2010).

[18]Y. Lu, H.-P. Chan, J. Wei, L. Hadjiiski, and C. Zhou, "Multiscale regularized reconstruction for enhancing microcalcification in digital breast tomosynthesis," Proc. SPIE **8313**, 831322–831329 (2012).

[19]Y. Chen, J. Y. Lo, and J. T. Dobbins III, "Impulse response analysis for several digital tomosynthesis mammography reconstruction algorithms," Proc. SPIE **5745**, 541–549 (2005).

[20]Y. Chen, J. Y. Lo, J. A. Baker, and J. T. Dobbins III, "Gaussian frequency blending algorithm with matrix inversion tomosynthesis (MITS) and filtered back projection (FBP) for better digital breast tomosynthesis reconstruction," Proc. SPIE **6142**, 61420E–61429E (2006).

[21]K. Lange and J. A. Fessler, "Globally convergent algorithms for maximum a posteriori transmission tomography," IEEE Trans. Image Process. **4**, 1430–1438 (1995).

[22]T. Wu, A. Stewart, M. Stanton, T. McCauley, W. Phillips, D. B. Kopans, R. H. Moore, J. W. Eberhard, B. Opsahl-Ong, L. Niklason, and M. B. Williams, "Tomographic mammography using a limited number of low-dose cone-beam projection images," Med. Phys. **30**, 365–380 (2003).

[23]T. Wu, J. Zhang, R. Moore, E. Rafferty, D. Kopans, W. Meleis, and D. Kaeli, "Digital tomosynthesis mammography using a parallel maximum-likelihood reconstruction method," Proc. SPIE **5368**, 1–11 (2004).

[24]I. Goddard, T. Wu, S. Thieret, A. Berman, and H. Bartsch, "Implementing an iterative reconstruction algorithm for digital breast tomosynthesis on graphics processing hardware," Proc. SPIE **6142**, 61424V–61427V (2006).

[25]G. Pratx and L. Xing, "GPU computing in medical physics: A review," Med. Phys. **38**, 2685–2697 (2011).

[26]G. Wu, J. Mainprize and M. Yaffe, "Characterization of projection ordering in iterative reconstruction methods for breast tomosynthesis," in *Proceedings of the 9th International Workshop on Digital Mammography* (Springer Berlin Heidelberg, Tucson, AZ, 2008), pp. 601–605.

[27]I. Kastanis, S. Arridge, A. Stewart, S. Gunn, C. Ullberg and T. Francke, "3D digital breast tomosynthesis using total variation regularization," in *Proceedings of the 9th International Workshop on Digital Mammography* (Springer Berlin Heidelberg, Tucson, AZ, 2008), pp. 621–627.

[28]E. Y. Sidky, I. S. Reiser, R. M. Nishikawa and X. Pan, "Preliminary study on the impact of digital breast tomosynthesis scanning angle on micro-calcification imaging," in *Proceedings of the IEEE Nuclear Science Symposium Conference Record* (IEEE, Dresden, Germany, 2008), pp. 4201–4204.

[29]E. Y. Sidky, X. Pan, I. S. Reiser, R. M. Nishikawa, R. H. Moore, and D. B. Kopans, "Enhanced imaging of microcalcifications in digital breast tomosynthesis through improved image-reconstruction algorithms," Med. Phys. **36**, 4920–4932 (2009).

[30]E. Y. Sidky, I. Reiser, R. M. Nishikawa, X. Pan, R. Chartrand, D. B. Kopans, and R. H. Moore, "Practical iterative image reconstruction in digital breast tomosynthesis by non-convex TpV optimization," Proc. SPIE **6913**, 691328 (2008).

[31]E. Y. Sidky, Y. Duchin, I. Reiser, C. Ullberg, and P. Xiaochuan, "Optimizing algorithm parameters based on a model observer detection task for image reconstruction in digital breast tomosynthesis," in *Proceedings of the IEEE Nuclear Science Symposium and Medical Imaging Conference (NSS/MIC)* (IEEE, Valencia, Spain, 2011), pp. 4230–4232.

[32]D. Van de Sompel and S. M. Brady, "Robust joint entropy regularization of limited view transmission tomography using Gaussian approximations to the joint histogram," in *Proceedings of the International Conference on Information Processing in Medical Imaging* (Springer Berlin Heidelberg, Williamsburg, VA, 2009), pp. 638–650.

[33]D. Van de Sompel and M. Brady, "Regularising limited view tomography using anatomical reference images and information theoretic similarity metrics," Med. Image Anal. **16**, 278–300 (2012).

[34]Y. Lu, H.-P. Chan, J. A. Fessler, L. Hadjiiski, J. Wei, and M. M. Goodsitt, "Adaptive diffusion regularization for enhancement of microcalcifications in digital breast tomosynthesis (DBT) reconstruction," Proc. SPIE **7961**, 796117 (2011).
[35]M. Das, H. C. Gifford, J. M. O'Connor, and S. J. Glick, "Penalized maximum likelihood reconstruction for improved microcalcification detection in breast tomosynthesis," IEEE Trans. Med. Imaging **30**, 904–914 (2011).
[36]A. Jerebko, M. Kowarschik, and T. Mertelmeier, "Regularization parameter selection in maximum a posteriori iterative reconstruction for digital breast tomosynthesis," in *Proceedings of the 10th International Workshop on Digital Mammography* (Springer Berlin Heidelberg, Girona, Spain, 2010), pp. 548–555.
[37]S. Xu and Y. Chen, "A Compton scattering suppression based image reconstruction method for digital breast tomosynthesis," in *Proceedings of the IEEE International Workshop on Genomic Signal Processing and Statistics (GENSIPS)* (IEEE, San Antonio, TX, 2011), pp. 190–193.
[38]G. Wu, J. Mainprize, and M. Yaffe, "Breast tomosynthesis reconstruction using a grid of blobs with projection matrices," in *Proceedings of the 10th International Workshop on Digital Mammography* (Springer Berlin Heidelberg, Girona, Spain, 2010), pp. 243–250.
[39]J. Chung, J. G. Nagy, and I. Sechopoulos, "Numerical algorithms for polyenergetic digital breast tomosynthesis reconstruction," SIAM J. Imaging Sci. **3**, 133–152 (2010).
[40]S. Suryanarayanan, A. Karellas, S. Vedantham, S. J. Glick, C. J. D'Orsi, S. P. Baker, and R. L. Webber, "Comparison of tomosynthesis methods used with digital mammography," Acad. Radiol. **7**, 1085–1097 (2000).
[41]S. Suryanarayanan, A. Karellas, S. Vedantham, S. P. Baker, S. J. Glick, C. J. D'Orsi, and R. L. Webber, "Evaluation of linear and nonlinear tomosynthetic reconstruction methods in digital mammography," Acad. Radiol. **8**, 219–224 (2001).
[42]T. Wu, R. H. Moore, E. A. Rafferty, and D. B. Kopans, "A comparison of reconstruction algorithms for breast tomosynthesis," Med. Phys. **31**, 2636–2647 (2004).
[43]Y. Chen, J. Y. Lo, and J. T. Dobbins III, "Noise power spectrum analysis for several digital breast tomosynthesis reconstruction algorithms," Proc. SPIE **6142**, 614259 (2006).
[44]L. Zhou, J. Oldan, P. Fisher, and G. Gindi, "Low-contrast lesion detection in tomosynthetic breast imaging using a realistic breast phantom," Proc. SPIE **6142**, 61425A (2006).
[45]J. T. Rakowski and M. J. Dennis, "A comparison of reconstruction algorithms for C-arm mammography tomosynthesis," Med. Phys. **33**, 3018–3032 (2006).
[46]Y. Zhang, H.-P. Chan, B. Sahiner, J. Wei, M. M. Goodsitt, L. M. Hadjiiski, J. Ge and C. Zhou, "A comparative study of limited-angle cone-beam reconstruction methods for breast tomosynthesis," Med. Phys. **33**, 3781–3795 (2006).
[47]Z. Kolitsi, G. Panayiotakis, V. Anastassopoulos, A. Scodras, and N. Pallikarakis, "A multiple projection method for digital tomosynthesis," Med. Phys. **19**, 1045–1050 (1992).
[48]Z. Kolitsi, G. Panayiotakis, and N. Pallikarakis, "A method for selective removal of out-of-plane structures in digital tomosynthesis," Med. Phys. **20**, 47–50 (1993).
[49]K. Bliznakova, Z. Kolitsi, R. D. Speller, J. A. Horrocks, G. Tromba, and N. Pallikarakis, "Evaluation of digital breast tomosynthesis reconstruction algorithms using synchrotron radiation in standard geometry," Med. Phys. **37**, 1893–1903 (2010).
[50]A. Balla, W. Zhou, and Y. Chen, "Impulse response characterization of breast tomosynthesis reconstruction with parallel imaging configurations," Proc. SPIE **7622**, 76225K (2010).
[51]D. Van de Sompel, S. M. Brady, and J. Boone, "Task-based performance analysis of FBP, SART and ML for digital breast tomosynthesis using signal CNR and channelised hotelling observers," Med. Image Anal. **15**, 53–70 (2011).
[52]T. Wu, R. H. Moore, and D. B. Kopans, "Voting strategy for artifact reduction in digital breast tomosynthesis," Med. Phys. **33**, 2461–2471 (2006).
[53]J. Ge, H.-P. Chan, B. Sahiner, Y. Zhang, J. Wei, L. M. Hadjiiski, and C. Zhou, "Digital tomosynthesis mammography: Intra- and interplane artifact reduction for high-contrast objects on reconstructed slices using a priori 3D geometrical information," Proc. SPIE **6512**, 65124Q–65128Q (2007).
[54]J. Ge, H.-P. Chan, B. Sahiner, Y. Zhang, J. Wei, L. M. Hadjiiski, C. Zhou, Y.-T. Wu, and J. Shi, "Digital tomosynthesis mammography: improvement of artifact reduction method for high-attenuation objects on reconstructed slices," Proc. SPIE **6913**, 69134O–69136O (2008).
[55]K. Erhard, M. Grass, and T. Nielsen, "A second pass correction method for calcification artifacts in digital breast tomosynthesis," Proc. SPIE **7961**, 796119 (2011).
[56]X. Sun, W. Land, and R. Samala, "Deblurring of tomosynthesis images using 3D anisotropic diffusion filtering," Proc. SPIE **6512**, 65124P (2007).
[57]Y. Zhang, H.-P. Chan, B. Sahiner, Y.-T. Wu, C. Zhou, J. Ge, J. Wei, and L. M. Hadjiiski, "Application of boundary detection information in breast tomosynthesis reconstruction," Med. Phys. **34**, 3603–3613 (2007).
[58]B. Li, G. Avinash, B. Claus, and S. Metz, "3D view weighted cone-beam backprojection reconstruction for digital tomosynthesis," Proc. SPIE **6510**, 65104X–65108X (2007).
[59]Y. Zhang, H. P. Chan, B. Sahiner, J. Wei, C. Zhou, and L. M. Hadjiiski, "Artifact reduction methods for truncated projections in iterative breast tomosynthesis reconstruction," J. Comput. Assist. Tomogr. **33**, 426–435 (2009).
[60]Y. Lu, H.-P. Chan, J. Wei, L. Hadjiiski, and C. Zhou, "Improving image quality of digital breast tomosynthesis by artifact reduction," in *Proceedings of the 11th International Workshop on Breast Imaging* (Springer Berlin Heidelberg, Philadelphia, PA, 2012), pp. 745–752.
[61]F. Diekmann, H. Meyer, S. Diekmann, S. Puong, S. Muller, U. Bick, and P. Rogalla, "Thick slices from tomosynthesis data sets: Phantom study for the evaluation of different algorithms," J. Digit Imaging **22**, 519–526 (2009).
[62]J. G. Mainprize, A. Bloomquist, X. Wang, and M. J. Yaffe, "Dependence of image quality on geometric factors in breast tomosynthesis," Med. Phys. **38**, 3090–3103 (2011).
[63]X. Li, Z. Da, and B. Liu, "A generic geometric calibration method for tomographic imaging systems with flat-panel detectors: A detailed implementation guide," Med. Phys. **37**, 3844–3854 (2010).
[64]X. Li, Z. Da and B. Liu, "Sensitivity analysis of a geometric calibration method using projection matrices for digital tomosynthesis systems," Med. Phys. **38**, 202–209 (2011).
[65]S. S. J. Feng and I. Sechopoulos, "Clinical digital breast tomosynthesis system: Dosimetric characterization," Radiology **263**, 35–42 (2012).
[66]M. L. Spangler, M. L. Zuley, J. H. Sumkin, G. Abrams, M. A. Ganott, C. Hakim, R. Perrin, D. M. Chough, R. Shah, and D. Gur, "Detection and classification of calcifications on digital breast tomosynthesis and 2D digital mammography: A comparison," Am. J. Roentgenol. **196**, 320–324 (2011).
[67]E. A. Rafferty, "Digital mammography: Novel applications," Radiol. Clin. North Am. **45**, 831–843 (2007).
[68]S. P. Poplack, T. D. Tosteson, C. A. Kogel, and H. M. Nagy, "Digital breast tomosynthesis: Initial experience in 98 women with abnormal digital screening mammography," Am. J. Roentgenol. **189**, 616–623 (2007).
[69]H. Teertstra, C. Loo, M. van den Bosch, H. van Tinteren, E. Rutgers, S. Muller, and K. Gilhuijs, "Breast tomosynthesis in clinical practice: Initial results," Eur. Radiol. **20**, 16–24 (2010).
[70]D. Kopans, S. Gavenonis, E. Halpern, and R. Moore, "Calcifications in the breast and digital breast tomosynthesis," Breast J. **17**, 638–644 (2011).
[71]M. G. Wallis, E. Moa, F. Zanca, K. Leifland, and M. Danielsson, "Two-view and single-view tomosynthesis versus full-field digital mammography: High-resolution x-ray imaging observer study," Radiology **262**, 788–796 (2012).
[72]G. Svane, E. Azavedo, K. Lindman, M. Urech, J. Nilsson, N. Weber, L. Lindqvist, and C. Ullberg, "Clinical experience of photon counting breast tomosynthesis: Comparison with traditional mammography," Acta Radiol. **52**, 134–142 (2011).
[73]I. Andersson, D. Ikeda, S. Zackrisson, M. Ruschin, T. Svahn, P. Timberg, and A. Tingberg, "Breast tomosynthesis and digital mammography: A comparison of breast cancer visibility and BIRADS classification in a population of cancers with subtle mammographic findings," Eur. Radiol. **18**, 2817–2825 (2008).
[74]D. Gur, M. L. Zuley, M. I. Anello, G. Y. Rathfon, D. M. Chough, M. A. Ganott, C. M. Hakim, L. Wallace, A. Lu, and A. I. Bandos, "Dose reduction in digital breast tomosynthesis (DBT) screening using synthetically reconstructed projection images: An observer performance study," Acad. Radiol. **19**, 166–171 (2012).
[75]D. Gur, University of Pittsburgh (personal communication).

[76]D. Kontos, P. R. Bakic, A.-K. Carton, A. B. Troxel, E. F. Conant, and A. D. A. Maidment, "Parenchymal texture analysis in digital breast tomosynthesis for breast cancer risk estimation: A preliminary study," Acad. Radiol. **16**, 283–298 (2009).
[77]D. Kontos, L. C. Ikejimba, P. R. Bakic, A. B. Troxel, E. F. Conant, and A. D. Maidment, "Analysis of parenchymal texture with digital breast tomosynthesis: Comparison with digital mammography and implications for cancer risk assessment," Radiology **261**, 80–91 (2011).
[78]D. Kontos, C. Zhang, N. Ruiter, P. Bakic, and A. Maidment, "Evaluating the effect of tomosynthesis acquisition parameters on image texture: A study based on an anthropomorphic breast tissue software model," in *Proceedings of the 9th International Workshop on Digital Mammography* (Springer Berlin Heidelberg, Tucson, AZ, 2008), pp. 491–498.
[79]E. Engstrom, I. Reiser, and R. Nishikawa, "Comparison of power spectra for tomosynthesis projections and reconstructed images," Med. Phys. **36**, 1753–1758 (2009).
[80]L. Chen, C. K. Abbey, A. Nosrateih, K. K. Lindfors, and J. M. Boone, "Anatomical complexity in breast parenchyma and its implications for optimal breast imaging strategies," Med. Phys. **39**, 1435–1441 (2012).
[81]Y.-H. Hu, M. Masiar, and W. Zhao, "Breast structural noise in digital breast tomosynthesis and its dependence on reconstruction methods," in *Proceedings of the 10th International Workshop on Digital Mammography* (Springer Berlin Heidelberg, Girona, Spain, 2010), pp. 598–605.
[82]A. E. Burgess and P. F. Judy, "Signal detection in power-law noise: Effect of spectrum exponents," J. Opt. Soc. Am. A **24**, B52–B60 (2007).
[83]P. R. Bakic, A.-K. Carton, D. Kontos, C. Zhang, A. B. Troxel, and A. D. A. Maidment, "Breast percent density: Estimation on digital mammograms and central tomosynthesis projections," Radiology **252**, 40–49 (2009).
[84]J. W. Byng, N. F. Boyd, E. Fishell, R. A. Jong, and M. J. Yaffe, "The quantitative analysis of mammographic densities," Phys. Med. Biol. **39**, 1629–1638 (1994).
[85]A. Tagliafico, G. Tagliafico, D. Astengo, F. Cavagnetto, R. Rosasco, G. Rescinito, F. Monetti, and M. Calabrese, "Mammographic density estimation: One-to-one comparison of digital mammography and digital breast tomosynthesis using fully automated software," Eur. Radiol. **22**, 1265–1270 (2012).
[86]P. R. Bakic, D. Kontos, A.-K. Carton, and A. D. A. Maidment, "Breast percent density estimation from 3D reconstructed digital breast tomosynthesis images," Proc. SPIE **6913**, 691318 (2008).
[87]N. Packard and J. M. Boone, "Glandular segmentation of cone beam breast CT volume images," Proc. SPIE **6510**, 651038 (2007).
[88]Z. Chen, "Histogram partition and interval thresholding for volumetric breast tissue segmentation," Comput. Med. Imaging Graph. **32**, 1–10 (2008).
[89]T. R. Nelson, L. I. Cervino, J. M. Boone, and K. K. Lindfors, "Classification of breast computed tomography data," Med. Phys. **35**, 1078–1086 (2008).
[90]X. Yang, I. Sechopoulos, and B. Fei, "Automatic tissue classification for high-resolution breast CT images based on bilateral filtering," Proc. SPIE **7962**, 79623H (2011).
[91]X. Yang, S. Wu, I. Sechopoulos, and B. Fei, "Bias correction and automated classification for high-resolution dedicated breast CT images," Med. Phys. **39**, 6397–6406 (2012).
[92]D. Kontos, R. Berger, P. R. Bakic, and A. D. A. Maidment, "Breast tissue classification in digital breast tomosynthesis images using texture features: A feasibility study," Proc. SPIE **7260**, 726024 (2009).
[93]S. Vedantham, L. Shi, A. Karellas, K. E. Michaelsen, V. Krishnaswamy, B. W. Pogue, and K. D. Paulsen, "Semi-automated segmentation and classification of digital breast tomosynthesis reconstructed images," in *Proceedings of the 33rd Annual International Conference of the IEEE Engineering in Medicine and Biology Society* (IEEE, Boston, 2011), pp. 6188–6191.
[94]S. Young, S. Park, S. K. Anderson, A. Badano, K. J. Myers, and P. Bakic, "Estimating breast tomosynthesis performance in detection tasks with variable-background phantoms," Proc. SPIE **7258**, 72580O–72589O (2009).
[95]S. Park, R. Jennings, H. Liu, A. Badano, and K. Myers, "A statistical, task-based evaluation method for three-dimensional x-ray breast imaging systems using variable-background phantoms," Med. Phys. **37**, 6253–6270 (2010).
[96]G. J. Gang, J. Lee, J. W. Stayman, D. J. Tward, W. Zbijewski, J. L. Prince, and J. H. Siewerdsen, "Analysis of Fourier-domain task-based detectability index in tomosynthesis and cone-beam CT in relation to human observer performance," Med. Phys. **38**, 1754–1768 (2011).
[97]I. Reiser, R. M. Nishikawa, M. L. Giger, T. Wu, E. Rafferty, R. H. Moore and D. B. Kopans, "Computerized detection of mass lesions in digital breast tomosynthesis images using two- and three dimensional radial gradient index segmentation," Technol. Cancer Res. Treat. **3**, 437–441 (2004).
[98]H.-P. Chan, J. Wei, B. Sahiner, E. A. Rafferty, T. Wu, M. A. Roubidoux, R. H. Moore, D. B. Kopans, L. M. Hadjiiski, and M. A. Helvie, "Computer-aided detection system for breast masses on digital tomosynthesis mammograms: Preliminary experience," Radiology **237**, 1075–1080 (2005).
[99]H.-P. Chan, J. Wei, Y. Zhang, B. Sahiner, L. Hadjiiski, and M. Helvie, "Detection of masses in digital breast tomosynthesis mammography: Effects of the number of projection views and dose," in *Proceedings of the 9th International Workshop on Digital Mammography* (Springer Berlin Heidelberg, Tucson, AZ, 2008), pp. 279–285.
[100]I. Reiser, R. M. Nishikawa, M. L. Giger, T. Wu, E. A. Rafferty, R. Moore, and D. B. Kopans, "Computerized mass detection for digital breast tomosynthesis directly from the projection images," Med. Phys. **33**, 482–491 (2006).
[101]H. P. Chan, J. Wei, Y. Zhang, M. A. Helvie, R. H. Moore, B. Sahiner, L. Hadjiiski, and D. B. Kopans, "Computer-aided detection of masses in digital tomosynthesis mammography: Comparison of three approaches," Med. Phys. **35**, 4087–4095 (2008).
[102]S. Singh, G. D. Tourassi, J. A. Baker, E. Samei, and J. Y. Lo, "Automated breast mass detection in 3D reconstructed tomosynthesis volumes: A featureless approach," Med. Phys. **35**, 3626–3636 (2008).
[103]M. A. Mazurowski, J. Y. Lo, B. P. Harrawood, and G. D. Tourassi, "Mutual information-based template matching scheme for detection of breast masses: From mammography to digital breast tomosynthesis," J. Biomed. Inf. **44**, 815–823 (2011).
[104]H. P. Chan, Y. T. Wu, B. Sahiner, J. Wei, M. A. Helvie, Y. Zhang, R. H. Moore, D. B. Kopans, L. Hadjiiski, and T. Way, "Characterization of masses in digital breast tomosynthesis: Comparison of machine learning in projection views and reconstructed slices," Med. Phys. **37**, 3576–3586 (2010).
[105]G. Peters, S. Muller, S. Bernard, R. Iordache, F. Wheeler, and I. Bloch, "Reconstruction-independent 3D CAD for calcification detection in digital breast tomosynthesis using fuzzy particles," in *Proceedings of the 10th Iberoamerican Congress on Pattern Recognition* (Springer Berlin Heidelberg, Havana, Cuba, 2005), pp. 400–408.
[106]I. Reiser, R. M. Nishikawa, A. V. Edwards, D. B. Kopans, R. A. Schmidt, J. Papaioannou, and R. H. Moore, "Automated detection of microcalcification clusters for digital breast tomosynthesis using projection data only: A preliminary study," Med. Phys. **35**, 1486–1493 (2008).
[107]S. C. Park, B. Zheng, X.-H. Wang, and D. Gur, "Applying a 2D based CAD scheme for detecting micro-calcification clusters using digital breast tomosynthesis images: An assessment," Proc. SPIE **6915**, 691507–691508 (2008).
[108]S. Bernard, S. Muller, and J. Onativia, "Computer-aided microcalcification detection on digital breast tomosynthesis data: A preliminary evaluation," in *Proceedings of the 9th International Workshop on Digital Mammography* (Springer Berlin Heidelberg, Tucson, AZ, 2008), pp. 151–157.
[109]B. Sahiner, H. P. Chan, L. M. Hadjiiski, M. A. Helvie, J. Wei, C. Zhou, and Y. Lu, "Computer-aided detection of clustered microcalcifications in digital breast tomosynthesis: A 3D approach," Med. Phys. **39**, 28–39 (2012).
[110]C. Ho, C. Tromans, J. Schnabel, and S. Brady, "A clustering method for the extraction of microcalcifications using epipolar curves in digital breast tomosynthesis," in *Proceedings of the 10th International Workshop on Digital Mammography* (Springer Berlin Heidelberg, Girona, Spain, 2010), pp. 682–688.
[111]C. Ho, C. Tromans, J. Schnabel, and S. Brady, "Microcalcification detection in digital breast tomosynthesis using an epipolar curve approach," in *Proceedings of the 10th International Workshop on Digital Mammography* (Springer Berlin Heidelberg, Girona, Spain, 2010), pp. 704–711.
[112]C. P. Ho, C. Tromans, J. A. Schnabel, and M. Brady, "Classification of clusters of microcalcifications in digital breast tomosynthesis," in *Proceedings of the 32nd Annual International Conference of the IEEE Engineering in Medicine and Biology Society* (IEEE, Buenos Aires, Argentina, 2010), pp. 3166–3169.
[113]P. Bakic, F. Richard, and A. Maidment, "Registration of mammograms and breast tomosynthesis images," in *Proceedings of the 8th*

International Workshop on Digital Mammography (Springer Berlin Heidelberg, Manchester, 2006), pp. 498–503.
[114]P. Bakic, F. Richard, and A. Maidment, "2D-to-3D x-ray breast image registration biomedical image registration," in *Proceedings of the 8th International Workshop on Digital Mammography* (Springer Berlin Heidelberg, Manchester, 2006), pp. 84–91.
[115]G. van Schie, C. Tanner, P. Snoeren, M. Samulski, K. Leifland, M. G. Wallis, and N. Karssemeijer, "Correlating locations in ipsilateral breast tomosynthesis views using an analytical hemispherical compression model," Phys. Med. Biol. **56**, 4715–4730 (2011).
[116]W. Zhang and S. Brady, "Feature point detection for non-rigid registration of digital breast tomosynthesis images," in *Proceedings of the 10th International Workshop on Digital Mammography* (Springer Berlin Heidelberg, Girona, Spain, 2010), pp. 296–303.
[117]S. P. Sinha, R. Narayanan, B. Ma, M. A. Roubidoux, H. Liu, and P. L. Carson, "Image registration for detection and quantification of change on digital tomosynthesis mammographic volumes," Am. J. Roentgenol. **192**, 384–387 (2009).
[118]G. Yang, J. Hipwell, M. Clarkson, C. Tanner, T. Mertzanidou, S. Gunn, S. Ourselin, D. Hawkes, and S. Arridge, "Combined reconstruction and registration of digital breast tomosynthesis," in *Proceedings of the 10th International Workshop on Digital Mammography* (Springer Berlin Heidelberg, Girona, Spain, 2010), pp. 760–768.
[119]C. M. Shafer, E. Samei, and J. Y. Lo, "The quantitative potential for breast tomosynthesis imaging," Med. Phys. **37**, 1004–1016 (2010).
[120]S. Richard and E. Samei, "Quantitative imaging in breast tomosynthesis and CT: Comparison of detection and estimation task performance," Med. Phys. **37**, 2627–2637 (2010).
[121]S. Richard and E. Samei, "Quantitative breast tomosynthesis: From detectability to estimability," Med. Phys. **37**, 6157–6165 (2010).
[122]M. D. Schnall *et al.*, "Diagnostic architectural and dynamic features at breast MR imaging: Multicenter study," Radiology **238**, 42–53 (2006).
[123]R. H. El Khouli, K. J. Macura, M. A. Jacobs, T. H. Khalil, I. R. Kamel, A. Dwyer, and D. A. Bluemke, "Dynamic contrast-enhanced MRI of the breast: Quantitative method for kinetic curve type assessment," Am. J. Roentgenol. **193**, W295–W300 (2009).
[124]R. H. El Khouli, K. J. Macura, I. R. Kamel, M. A. Jacobs, and D. A. Bluemke, "3-T dynamic contrast-enhanced MRI of the breast: Pharmacokinetic parameters versus conventional kinetic curve analysis," Am. J. Roentgenol. **197**, 1498–1505 (2011).
[125]R. H. El Khouli, K. J. Macura, P. B. Barker, M. R. Habba, M. A. Jacobs, and D. A. Bluemke, "Relationship of temporal resolution to diagnostic performance for dynamic contrast enhanced MRI of the breast," J. Magn. Reson Imaging **30**, 999–1004 (2009).
[126]A.-K. Carton, J. Li, M. Albert, S. Chen, and A. D. A. Maidment, "Quantification for contrast-enhanced digital breast tomosynthesis," Proc. SPIE **6142**, 61420D (2006).
[127]S. C. Chen, A. K. Carton, M. Albert, E. F. Conant, M. D. Schnall, and A. D. Maidment, "Initial clinical experience with contrast-enhanced digital breast tomosynthesis," Acad. Radiol. **14**, 229–238 (2007).
[128]S. J. Glick and C. Didier, "A computer simulation for evaluating dual-energy, contrast-enhanced breast tomosynthesis," Proc. SPIE **6510**, 65102V–65107V (2007).
[129]S. Puong, X. Bouchevreau, F. Patoureaux, R. Iordache, and S. Muller, "Dual-energy contrast enhanced digital mammography using a new approach for breast tissue canceling," Proc. SPIE **6510**, 65102H–65112H (2007).
[130]S. Puong, F. Patoureaux, R. Iordache, X. Bouchevreau, and S. Muller, "Dual-energy contrast enhanced digital breast tomosynthesis: concept, method, and evaluation on phantoms," Proc. SPIE **6510**, 65100U–65112U (2007).
[131]S. Puong, X. Bouchevreau, N. Duchateau, R. Iordache, and S. Muller, "Optimization of beam parameters and iodine quantification in dual-energy contrast enhanced digital breast tomosynthesis," Proc. SPIE **6913**, 69130Z (2008).
[132]R. Iordache, M. Lohezic, G. Palma, S. Puong, and S. Muller, "Noise reduction in dual-energy contrast enhanced digital breast tomosynthesis using regularization," in *Proceedings of the 10th International Workshop on Digital Mammography* (Springer Berlin Heidelberg, Girona, Spain, 2010), pp. 92–99.
[133]A.-K. Carton, J. A. Currivan, E. Conant, and A. Maidment, "Temporal subtraction versus dual-energy contrast-enhanced digital breast tomosynthesis: A pilot study," in *Proceedings of the 9th International Workshop on Digital Mammography* (Springer Berlin Heidelberg, Tucson, AZ, 2008), pp. 166–173.
[134]A. K. Carton, S. C. Gavenonis, J. A. Currivan, E. F. Conant, M. D. Schnall, and A. D. Maidment, "Dual-energy contrast-enhanced digital breast tomosynthesis: A feasibility study," Br. J. Radiol. **83**, 344–350 (2010).
[135]A.-K. Carton, C. Ullberg, K. Lindman, R. Acciavatti, T. Francke, and A. D. A. Maidment, "Optimization of a dual-energy contrast-enhanced technique for a photon-counting digital breast tomosynthesis system: I. A theoretical model," Med. Phys. **37**, 5896–5907 (2010).
[136]A.-K. Carton, C. Ullberg, and A. D. A. Maidment, "Optimization of a dual-energy contrast-enhanced technique for a photon-counting digital breast tomosynthesis system: II. An experimental validation," Med. Phys. **37**, 5908–5913 (2010).
[137]E. Samei and R. S. Saunders, "Dual-energy contrast-enhanced breast tomosynthesis: Optimization of beam quality for dose and image quality," Phys. Med. Biol. **56**, 6359–6378 (2011).
[138]F. F. Schmitzberger, E. M. Fallenberg, R. Lawaczeck, M. Hemmendorff, E. Moa, M. Danielsson, U. Bick, S. Diekmann, A. Pollinger, F. J. Engelken, and F. Diekmann, "Development of low-dose photon-counting contrast-enhanced tomosynthesis with spectral imaging," Radiology **259**, 558–564 (2011).
[139]E. Fredenberg, M. Lundqvist, M. Aslund, M. Hemmendorff, B. Cederstrom, and M. Danielsson, "A photon-counting detector for dual-energy breast tomosynthesis," Proc. SPIE **7258**, 72581J (2009).
[140]M. Hill, J. Mainprize, and M. Yaffe, "Sensitivity of contrast-enhanced digital breast tomosynthesis to changes in iodine concentration during acquisition," in *Proceedings of the 9th International Workshop on Digital Mammography* (Springer Berlin Heidelberg, Tucson, AZ, 2008), pp. 643–650.
[141]M. L. Hill, J. G. Mainprize, S. Puong, A.-K. Carton, R. Iordache, S. Muller, and M. J. Yaffe, "Impact of image acquisition timing on image quality for dual energy contrast-enhanced breast tomosynthesis," Proc. SPIE **8313**, 831308–831309 (2012).
[142]G. Boverman, T. J. Kao, R. Kulkarni, B. S. Kim, D. Isaacson, G. J. Saulnier, and J. C. Newell, "Robust linearized image reconstruction for multifrequency EIT of the breast," IEEE Trans. Med. Imaging **27**, 1439–1448 (2008).
[143]T. J. Kao, G. Boverman, D. Isaacson, G. J. Saulnier, J. C. Newell, R. H. Moore, and D. B. Kopans, "Regional admittivity spectra with tomosynthesis images for breast cancer detection," in *Proceedings of the 29th Annual International Conference of the IEEE Engineering in Medicine and Biology Society* (IEEE, Shanghai, China, 2007), pp. 4142–4145.
[144]T. J. Kao, G. Boverman, B. S. Kim, D. Isaacson, G. J. Saulnier, J. C. Newell, M. H. Choi, R. H. Moore, and D. B. Kopans, "Regional admittivity spectra with tomosynthesis images for breast cancer detection: Preliminary patient study," IEEE Trans. Med. Imaging **27**, 1762–1768 (2008).
[145]S. P. Sinha, M. A. Roubidoux, M. A. Helvie, A. V. Nees, M. M. Goodsitt, G. L. LeCarpentier, J. B. Fowlkes, C. L. Chalek, and P. L. Carson, "Multimodality 3D breast imaging with x-ray tomosynthesis and automated ultrasound," in *Proceedings of the 29th Annual International Conference of the IEEE Engineering in Medicine and Biology Society* (IEEE, Shanghai, China, 2007), pp. 1335–1338.
[146]A. Kapur *et al.*, "Combination of digital mammography with semi-automated 3D breast ultrasound," Technol. Cancer Res. Treat. **3**, 325–334 (2004).
[147]M. J. More, L. Heng, P. J. Goodale, Z. Yibin, S. Majewski, V. Popov, B. Welch, and M. B. Williams, "Limited angle dual modality breast imaging," IEEE Trans. Nucl. Sci. **54**, 504–513 (2007).
[148]M. Williams *et al.*, "Tomographic dual modality breast scanner," in *Proceedings of the 9th International Workshop on Digital Mammography* (Springer Berlin Heidelberg, Tucson, AZ, 2008), pp. 99–107.
[149]M. B. Williams, P. G. Judy, S. Gunn, and S. Majewski, "Dual-modality breast tomosynthesis," Radiology **255**, 191–198 (2010).
[150]G. Boverman, Q. Fang, S. A. Carp, E. L. Miller, D. H. Brooks, J. Selb, R. H. Moore, D. B. Kopans, and D. A. Boas, "Spatio-temporal imaging of the hemoglobin in the compressed breast with diffuse optical tomography," Phys. Med. Biol. **52**, 3619–3641 (2007).
[151]Q. Fang, R. H. Moore, D. B. Kopans, and D. A. Boas, "Compositional-prior-guided image reconstruction algorithm for multi-modality imaging," Biomed. Opt. Express **1**, 223–235 (2010).
[152]Q. Fang, J. Selb, S. A. Carp, G. Boverman, E. L. Miller, D. H. Brooks, R. H. Moore, D. B. Kopans, and D. A. Boas, "Combined

optical and x-ray tomosynthesis breast imaging," Radiology **258**, 89–97 (2011).
[153]S. W. Wilkins, T. E. Gureyev, D. Gao, A. Pogany, and A. W. Stevenson, "Phase-contrast imaging using polychromatic hard x-rays," Nature (London) **384**, 335–338 (1996).
[154]C. Honda and H. Ohara, "Advantages of magnification in digital phase-contrast mammography using a practical x-ray tube," Eur. J. Radiol. **68**, S69–S72 (2008).
[155]X. Tang, Y. Yang, and S. Tang, "Characterization of imaging performance in differential phase contrast CT compared with the conventional CT: Noise power spectrum NPS(k)," Med. Phys. **38**, 4386–4395 (2011).
[156]J. C. Hammonds, R. R. Price, E. F. Donnelly, and D. R. Pickens, "Phase-contrast digital tomosynthesis," Med. Phys. **38**, 2353–2358 (2011).
[157]G. W. Kim, B. H. Han, M. H. Cho, and S. Y. Lee, "X-ray elastography: A feasibility study," in *Proceedings of the 31st Annual International Conference of the IEEE Engineering in Medicine and Biology Society* (IEEE, Minneapolis, 2009), pp. 3513–3516.
[158]F. J. Engelken, I. Sack, D. Klatt, T. Fischer, E. M. Fallenberg, U. Bick, and F. Diekmann, "Evaluation of tomosynthesis elastography in a breast-mimicking phantom," Eur. J. Radiol. **81**, 2169–2173 (2012).
[159]Y. Lyatskaya, A. Buehler, S. K. Ng, J. Wong, J. R. Bellon, and P. Zygmanski, "Optimal gantry angles and field sizes in kilovoltage cone-beam tomosynthesis for set-up of women with breast cancer undergoing radiotherapy treatment," Radiother. Oncol. **93**, 633–638 (2009).
[160]B. A. Winey, P. Zygmanski, R. A. Cormack, and Y. Lyatskaya, "Balancing dose and image registration accuracy for cone beam tomosynthesis (CBTS) for breast patient setup," Med. Phys. **37**, 4414–4423 (2010).
[161]J. Zhang, Q. J. Wu, D. J. Godfrey, T. Fatunase, L. B. Marks, and F. F. Yin, "Comparing digital tomosynthesis to cone-beam CT for position verification in patients undergoing partial breast irradiation," Int. J. Radiat. Oncol., Biol., Phys. **73**, 952–957 (2009).
[162]S. K. Ng, P. Zygmanski, A. Jeung, H. Mostafavi, J. Hesser, J. R. Bellon, J. S. Wong, and Y. Lyatskaya, "Optimal parameters for clinical implementation of breast cancer patient setup using Varian DTS software," J. Appl. Clin. Med. Phys. **13**, 60–73 (2012).
[163]V. Sarkar, C. Shi, P. Rassiah-Szegedi, A. Diaz, T. Eng, and N. Papanikolaou, "The effect of a limited number of projections and reconstruction algorithms on the image quality of megavoltage digital tomosynthesis," J. Appl. Clin. Med. Phys. **10**, 155–172 (2009).
[164]B. Winey, P. Zygmanski, and Y. Lyatskaya, "Evaluation of radiation dose delivered by cone beam CT and tomosynthesis employed for setup of external breast irradiation," Med. Phys. **36**, 164–173 (2009).
[165]D. J. Godfrey, L. Ren, H. Yan, Q. Wu, S. Yoo, M. Oldham, and F. F. Yin, "Evaluation of three types of reference image data for external beam radiotherapy target localization using digital tomosynthesis (DTS)," Med. Phys. **34**, 3374–3384 (2007).